

# **The impact of observation nudging on simulated meteorology and ozone concentrations during DISCOVER-AQ 2013 Texas campaign**

Xiangshang Li <sup>1</sup>, Yunsoo Choi <sup>1</sup>, Beata Czader <sup>1</sup>, Hyuncheol Kim <sup>2,3</sup>, Barry Lefer <sup>1</sup>, Shuai Pan <sup>1</sup>

<sup>1</sup>Department of Earth and Atmospheric Sciences, University of Houston, Houston, TX, 77204, USA

<sup>2</sup>NOAA Air Resources Laboratory, College Park, MD 20740, USA

<sup>3</sup>University of Maryland, Cooperative Institute for Climate and Satellite, College Park, MD, USA

Corresponding author: Xiangshang Li: xli@central.uh.edu

## **Abstract**

Air quality modeling demands accurate meteorological simulations. Observation nudging (here in conjunction with objective analysis) is generally considered a low-cost and effective technique to improve meteorological simulations. However the meteorological impact of observation nudging on chemistry has not been well characterized. This study involved two simulations to analyze the impact of observation nudging on the simulated meteorology and ozone concentrations during the Deriving Information on Surface conditions from Column and Vertically Resolved Observations Relevant to Air Quality (DISCOVER-AQ) Texas campaign period in September 2013, using Weather Research and Forecasting (WRF) and Community Multiscale Air Quality (CMAQ) models. The results showed improved correlations between observed and simulated parameters from the sensitivity case. The index of agreement (IOA) improved by about 9% for surface temperature and 6-11% for surface zonal (U-WIND) and meridional (V-WIND) winds when observation nudging was employed. Analysis of a cold front event indicated that it improved the timing of wind transition during front passage. Employing observation nudging also reduced the model biases in the planetary boundary height predictions.

27 For CMAQ simulated surface ozone during the whole simulated period, IOA improved by 6% in  
28 the sensitivity case. The high ozone episode on September 25<sup>th</sup> was a typical post-front ozone  
29 event in Houston. The small-scale morning wind-shifts near the Houston Ship Channel combined  
30 with higher aloft ozone early morning likely caused the day's ozone exceedance. While  
31 observation nudging did not reproduce the wind shifts on that day and failed to reproduce the  
32 observed surface and aloft high ozone, analyses of surface and aircraft data found that  
33 observation nudging results matched better with observations. In a two-hour period during the  
34 event, substantially better winds in the sensitivity case noticeably improved the ozone. Further  
35 work on improving its capability to reproduce local meteorological events could enhance a  
36 chemistry model's ability to predict high ozone events.

37 **Keywords:** WRF, CMAQ, air quality model, DISCOVER-AQ, observation nudging

38

## 39 **1. Introduction**

40 Accurate meteorological simulations are essential to photochemical modeling since  
41 meteorological variables, such as cloud fraction, winds, planetary boundary layer (PBL) heights  
42 and precipitation, significantly impact the production, transport, and deposition of various  
43 chemical species (e.g., Pour-Biazar et al 2007; Banta et al. 2005; Cuchiara et al. 2014). Common  
44 approaches of improving meteorological simulations include the selection of high quality terrain  
45 and input data (e.g., Cheng and Byun 2008), the optimization of physics and dynamics options  
46 (e.g., Zhong et al. 2007), and the implementation of four dimensional data assimilation (FDDA).  
47 The air quality modeling group at the University of Houston (UH) had performed several  
48 sensitivity studies on the various parameterization schemes in the recent past (e.g. Zhong et al.  
49 2007; Ngan et al. 2012; Cuchiara et al. 2014).

50 There are several FDDA methods including nudging (e.g., Stauffer and Seaman 2004) and  
51 Variational Methods (3D-VAR or 4D-VAR; e.g., Le Dimet and Talagrand 1986; Huang et al.  
52 2009). 4D-VAR obtains optimal states of the atmosphere using multi-time-level observations by  
53 globally adjusting a model solution to all available observations over an interval of time.  
54 Nudging is a simple yet flexible FDDA method originally developed by Stauffer and Seaman  
55 (1990, 1994), and implemented in the Fifth-Generation PSU/NCAR Mesoscale Model (MM5).

56 Not intended for optimal adjustment, nudging is less computationally intensive and needs special  
57 care for the nudging coefficients. Nudging involves adding an artificial tendency term to one or  
58 more model prognostic equations that reflect the difference between the best estimate of the  
59 observed state and the model state at a given location and time. In short, the goal is to “nudge”  
60 model state towards observed state. There are several types of nudging such as 3D analysis  
61 nudging, surface analysis nudging, and observation nudging (obs-nudging). In the case of  
62 analysis nudging, the model state is nudged toward gridded analysis. The difference between 3D  
63 and surface analysis nudging is that 3D analysis (at all model levels except for surface) data are  
64 used to improve 3D fields while surface analysis data are used to improve surface fields. In  
65 observation nudging, the model is perturbed such that its predictions match better with  
66 observations at individual locations, both on surface and aloft. The MM5 nudging codes were  
67 later improved and incorporated into the Weather Research and Forecasting (WRF) model by  
68 Liu et al. (2005, 2006). The enhancements enable obs-nudging to assimilate a large variety of  
69 direct or derived observations. In WRF, the input for obs-nudging are generated by WRF  
70 OBSGRID program. OBSGRID also performs Objective Analysis, or OA. Since obs-nudging is  
71 usually performed along with OA (as in this study) to maximize the benefits of assimilating  
72 observations, we also use OA to denote the combined Objective Analysis and obs-nudging  
73 processes in case names.

74 The benefit of applying nudging to improve meteorological simulations has been demonstrated  
75 in many studies (e.g., Deng 2009; Gilliam and Pleim 2010). However, only a few have extended  
76 the investigation into chemistry simulations. Otte (2008) showed that analysis nudging is able to  
77 improve MM5 meteorology, as well as Community Multiscale Air Quality (CMAQ) chemistry  
78 as reflected in ozone statistics. Better “model skill” scores were achieved for daily maximum 1-  
79 hr ozone mixing ratio after analysis nudging over a 35-day period. Byun et al. (2008) performed  
80 over a dozen tests on obs-nudging (with analysis nudging turned on) and showed obs-nudging  
81 improved both winds and temperature in MM5 simulations. The study also gave an example in  
82 which improved wind fields on a given day led CMAQ to better capture the high ozone area  
83 southwest of Houston. Ngan et al. (2012) compared results from several MM5-CMAQ  
84 simulations and showed that fully nudged (with both analysis nudging and obs-nudging  
85 implemented) simulations outperformed a forecast run in both meteorology and chemistry.  
86 However, the statistics from their study cannot be used for interpreting the sensitivity of obs-

87 nudging since its base WRF case is a forecast run which used a different analysis input. Previous  
88 by the current authors (e.g., Rappenglueck et al. 2011; Czader et al. 2013) showed that obs-  
89 nudging helps to correct errors in model wind fields, which are critical to the transport process of  
90 air pollutants, as well as the production of secondary pollutants. To the best of the authors'  
91 knowledge, there is no comprehensive existing study on the impact of obs-nudging on chemistry,  
92 especially when the meteorological model is WRF. This study intends to fill up the gap by  
93 investigating the sensitivity of WRF-CMAQ simulations to the use of observation nudging.  
94 Although not elaborated here, the WRF-CMAQ sensitivity to different obs-nudging frequencies  
95 was also explored. In theory, higher frequency of obs-nudging input should have a higher  
96 probability to capture small scale events, such as local wind shifts. These events may only  
97 slightly impact local weather, yet they can have a large effect on chemistry since it is well-  
98 known that local stagnation and wind convergence/reversals can contribute to the pollutant build-  
99 up (e.g., Banta et al. 1998; Cheung and Wang 2001; Tucker et al. 2010).

100 There is a significant presence of petro-chemical facilities, power plants and motor vehicles in  
101 the Houston-Galveston-Brazoria (HGB) region located in southeastern Texas (SETX). The major  
102 pollutant in the region is ozone due to the abundant emissions of precursors like nitrogen oxide  
103 ( $\text{NO}_x$ ) and Volatile Organic Compounds (VOCs). During the long and hot summer, ozone often  
104 rises above the threshold level as stipulated in the National Ambient Air Quality Standards  
105 (NAAQS). Consequently HGB has been designated as an ozone non-attainment region by the US  
106 Environmental Protection Agency (USEPA). The petro-chemical plants are largely concentrated  
107 in the Houston Ship Channel (HSC) area - just north of the Galveston Bay. The VOCs emitted  
108 from the HSC area are highly reactive and have been shown to contribute greatly to the high  
109 ozone episodes in HGB (e.g. Kleinman et al. 2002; Daum et al. 2003). Depending on the local  
110 meteorology, the plumes from HSC may be carried to different locations in HGB and trigger  
111 high ozone events on its path. Metropolitan Houston has a high level of  $\text{NO}_x$  emissions partly  
112 due to heavy vehicular traffic in the city. As a result of the large amount of precursor emissions  
113 and favorable weather, relatively frequent high ozone events occur in the area. Ngan and Byun  
114 (2011) gave an analysis on the relationships between the high ozone frequency and underlying  
115 weather patterns. They derived the weather patterns from a classification scheme using large-  
116 scale 850-hPa synoptic flow as input.

117 The Houston-Galveston-Brazoria region has been the location of interest of many air quality  
118 studies (e.g., Banta et al. 2005; Parrish et al. 2009; Lefer and Rappengluck 2010; Olaguer et al.  
119 2013; Czader et al. 2013, Choi et al. 2012; Choi 2014; Choi and Souri, 2015; Pan et al. 2015). It  
120 is a good place for studying ozone production and transport due to the existence of a dense  
121 surface monitoring network, as well as several intensive measurement field campaigns which  
122 provide ample observational data. For example, in September 2013, the National Aeronautics  
123 and Space Administration (NASA), joined by a number of agencies and universities, conducted a  
124 field measurement campaign in SETX as part of its the Deriving Information on Surface  
125 conditions from Column and Vertically Resolved Observations Relevant to Air Quality  
126 (DISCOVER-AQ) program. The NASA program has conducted air quality and meteorology  
127 measurements at several different locations in the U.S. The availability of dense surface  
128 observations is important for obs-nudging to correct erroneous local winds in the model. Without  
129 a rich set of observations, the performance of obs-nudging will be handicapped.

130 This study involved performing two WRF-CMAQ simulations for the 2013 DISCOVER-AQ  
131 Texas time period in order to understand the impact of obs-nudging using comprehensive sets of  
132 observation data from both in-situ surface and aircraft measurements. We evaluated model  
133 performance and calculated statistics for both WRF and CMAQ. Meteorological fields critical to  
134 ozone chemistry were examined to explore the model sensitivity to obs-nudging. The paper is  
135 structured as following: Section 1 is introduction; Section 2 describes the measurement data and  
136 the modeling system; Section 3 covers the evaluation protocols; Section 4 discusses the general  
137 meteorological conditions during the campaign period; Section 5 presents the modeling results,  
138 and Section 6 provides discussions and conclusions.

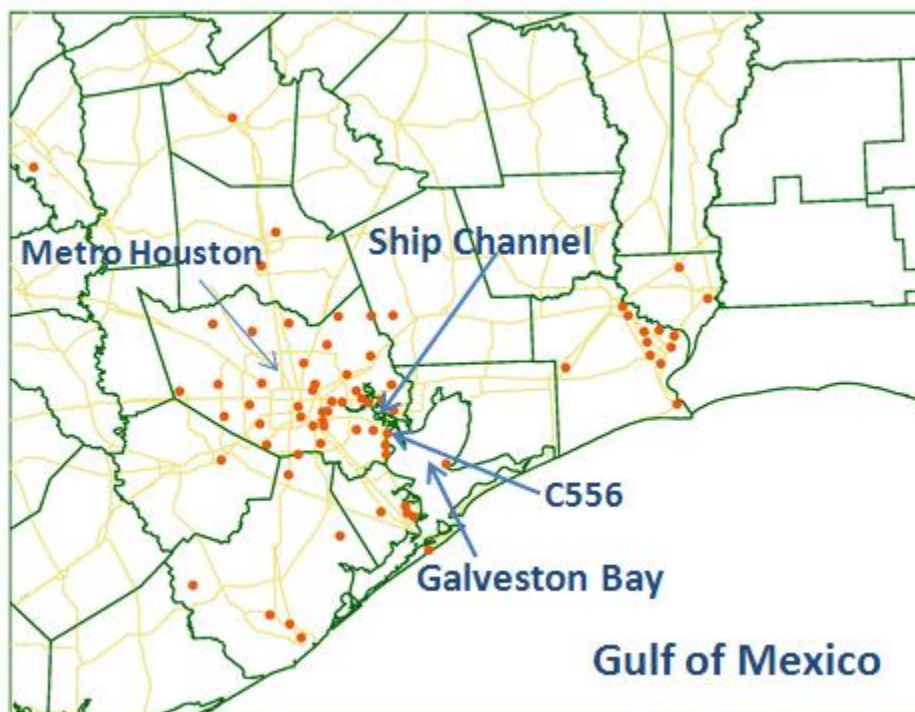
139

## 140 **2. Observational Data and Model Configurations**

141 For evaluation of the results, this study used regular measurements from the Continuous Ambient  
142 Monitoring Station (CAMS), operated by the Texas Commission on Environmental Quality  
143 (TCEQ), as well as PBL and aloft ozone measurements from DISCOVER-AQ campaign. For  
144 observation nudging, in addition to the CAMS data sets, several datastreams from the  
145 Meteorological Assimilation Data Ingest System (MADIS) were also used.

146 **2.1 Observational Data**

147 The CAMS measurement network collected real-time meteorology and chemistry data. The  
148 measured parameters differ from station to station. The station density at SETX is relatively  
149 high. There are 63 sites having meteorological measurements and 52 sites having ozone  
150 measurements in 4-km domain (Figure 1) during DISCOVER-AQ time period. The stations are  
151 represented by dots, with La Porte (C556) site labeled. All CAMS observations are accessible at  
152 TCEQ website: [http://www.tceq.state.tx.us/cgi-bin/compliance/monops/daily\\_summary.pl](http://www.tceq.state.tx.us/cgi-bin/compliance/monops/daily_summary.pl).



153  
154  
155 **Figure 1.** Locations of CAMS sites (dots) in CMAQ 4-km modeling domain during September  
156 2013. Metro Houston, Houston Ship Channel, Galveston Bay and Gulf of Mexico are labeled.

157 Additionally, PBL height measurements for September were obtained from a team at University  
158 of Houston, which employed LIDAR (Light Detection and Ranging) to detect the PBL height.  
159 Presently, only data at one site is available.

160 For analysis of ozone aloft on September 25, we also used measurements from aircraft P-3B, part  
161 of the rich datasets collected during DISCOVER-AQ campaign (<http://www->

162 [air.larc.nasa.gov/missions/discover-aq/discover-aq.html](http://air.larc.nasa.gov/missions/discover-aq/discover-aq.html)). The P-3B data had over 100  
163 parameters and are accessible from the website.

## 164 **2.2 Model Configurations**

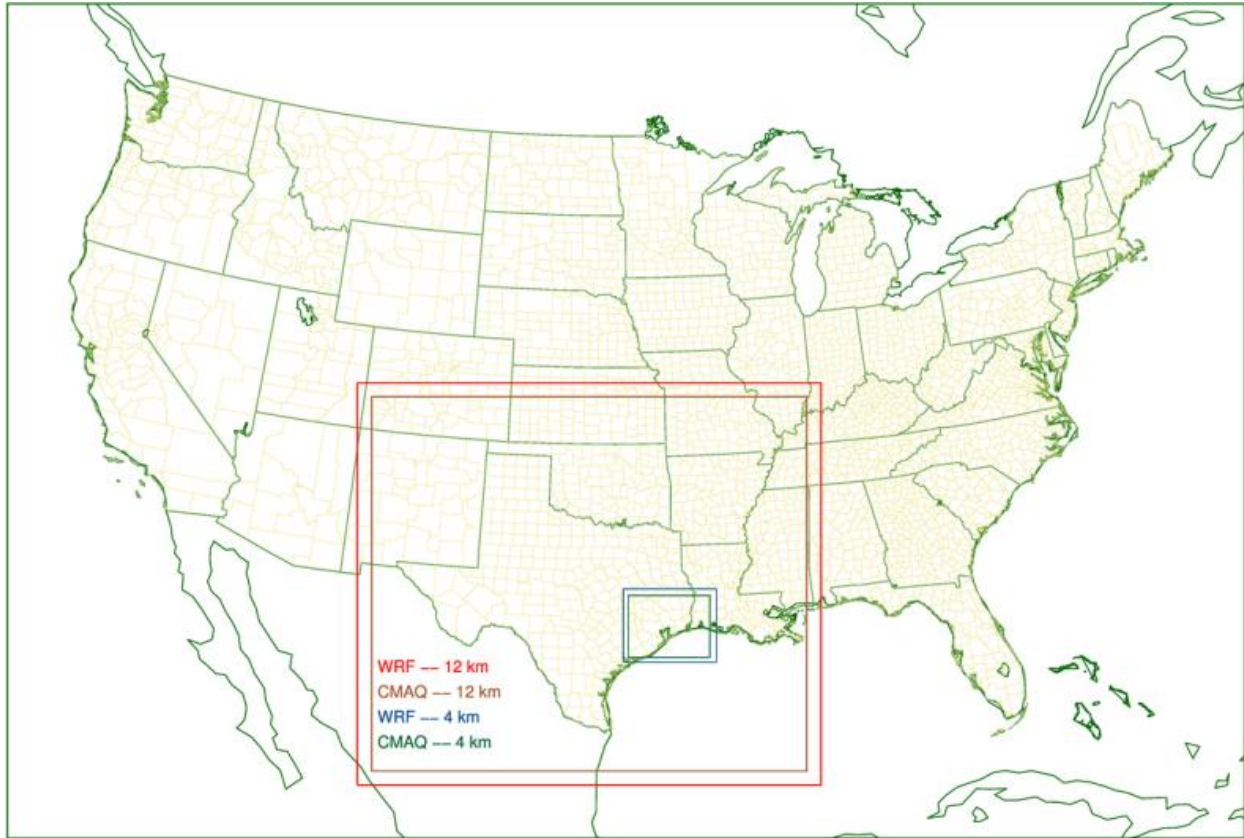
165 The modeling system consists of WRF-SMOKE-CMAQ models as described in the following  
166 three subsections. Two sets of simulations, with the only difference in whether obs-nudging and  
167 OA were included, were performed. The base case, referred as “No-OA”, did not employ  
168 observation nudging or OA. The second case, “1Hr-OA”, performed obs-nudging and OA using  
169 hourly observation nudging input.

### 170 **2.2.1. WRF Configurations**

171 Both WRF simulations used the same nested domain and NARR (North American Regional  
172 Reanalysis) as input, with grid nudging turned on.

#### 173 **2.2.1.1. Domain Setup**

174 Figure 2 depicts the horizontal domain setup. There were two nested domains, with 12-km and 4-  
175 km resolution. The 4-km domain covered SETX and a small portion of Louisiana. The 12-km  
176 domain (red box) encompassed Texas and a few neighboring states (or parts). The grid sizes for  
177 the 12-km and 4-km domains were 161 × 145 (E-W by N-S), and 95 × 77 respectively. The  
178 projection type is Lambert conic conformal (LCC). Three projection parameters, first latitude,  
179 the second latitude and the standard longitude, are 33 °N, 45 °N and 97 °W degrees respectively.  
180 The USEPA used the same projection parameters to develop emission inventories for air quality  
181 modeling. Vertically both domains had 27 eta layers based on dry hydrostatic pressures. The  
182 model top is set to be 100 hPa, corresponding to top layer pressure of the input NARR data.



183

184 **Figure 2.** Horizontal domains of WRF and CMAQ simulation at 4km and 12km grid resolution  
 185 (the bigger domains are for 12km WRF and CMAQ and the smaller domains for 4km WRF and  
 186 CMAQ).

187 **2.2.1.2. Input Data**

188 Both WRF simulations were retrospective runs using NARR analysis as input, downloadable  
 189 from: <http://rda.ucar.edu/datasets/ds608.0/>. The NARR data were based on an Eta 221 grid at 29  
 190 pressure levels. Its horizontal resolution was 32-km and the frequency was 3-hourly. The initial  
 191 and boundary conditions were generated from the NARR analysis by WRF. An alternative to  
 192 NARR was the Eta-NAM analysis data. However, the data temporal frequency was lowered  
 193 from 3-hourly to 6-hourly starting 2013. Our test showed that it was not as good as NARR for  
 194 WRF input, likely because of lower temporal resolution.

195 **2.2.1.3. Physics and FDDA Options**

196 Major physics options were listed in Table 1. These options are consistent with the WRF options  
197 in our daily air quality forecasting system (<http://spock.geosc.uh.edu/>). Among them, the PBL  
198 and cumulous cloud schemes are especially critical. Our past experiences demonstrated that  
199 Yonsei University (YSU) is the best PBL scheme in Houston case study while Kain-Fritsch (K-  
200 F) is the preferable cumulous scheme. The choice of YSU scheme is also corroborated recently  
201 by Cuchiara (2014) et al.. K-F scheme is “drier” than others and produces less bogus  
202 convectional thunderstorms. The numbers in parentheses represent the value of corresponding  
203 namelist variable in WRF’s namelist file. For example, the “1” after YSU is the value of the  
204 namelist variable “bl\_pbl\_physics” in WRF’s namelist file. For both of the simulations, we  
205 performed standard grid nudging for both of the cases using NARR analysis. For grid nudging  
206 options, we generally followed the recommendations in WRF’s User Guide. For example, the  
207 mass fields (temperature and moisture) were nudged only at layers above the PBL while wind  
208 fields were adjusted at all layers including the surface layer.

#### 209 **2.2.1.4. Observation Nudging with MADIS and CAMS data in WRF**

210 Additional observational data are required to implement obs-nudging and OA. In this study, we  
211 acquired the input observation data and generating files in “little\_r” format using similar  
212 procedures found in Ngan et al. (2012) and Czader et al. (2013). Observational data came from  
213 the MADIS and TCEQ CAMS. MADIS (<https://madis.ncep.noaa.gov/>), a National Oceanic and  
214 Atmospheric Administration (NOAA) program, collects, integrates, quality-controls, and  
215 distributes observations from NOAA and other organizations. The four MADIS datasets used for  
216 obs-nudging were NOAA Profiler Network (NPN), Cooperative Agency Profilers (CAP),  
217 Meteorological Terminal Aviation Routine (METAR) weather report and NOAA Radiosonde  
218 (RAOB). The METAR dataset was collected by mostly first-order, METAR reporting, surface  
219 monitoring stations. NPN, RAOB and CAP were the most commonly used upper air datasets.

220 The “little\_r” files from previous step were fed into WRF OBSGRID module to update the  
221 domain analyses (“met\_em” files), and, generate additional surface analyses (“sffdda”) and text  
222 nudging files (“OBS\_DOMAIN”). Actual obs-nudging was performed by the main WRF  
223 program after obs-nudging namelist variables are properly set. The namelist for OBSGRID and  
224 relevant WRF section settings came largely from recommended values of WRF User’s Guide  
225 and a previous study by Ngan et al. (2012).

226 Theoretically, obs-nudging updating at a higher frequency should enhance the model's  
227 performance. A typical frequency of input analysis data is 3-hourly while the frequency for  
228 observational data is hourly. The 3-hourly frequency of input analyses may be the reason for the  
229 default 3-hour time-interval in WRF's OBSGRID settings for generating the obs-nudging files.  
230 Since there were few existing obs-nudging studies related to air quality and we are not aware of  
231 any reference to the adoption of 1-hour input frequency, we assume that all the existing studies  
232 used the default 3-hour interval. As the WRF model allows the interval to be set to 1-hour or  
233 smaller when corresponding observational data were available, we tested both 1-hour and 3-hour  
234 scenarios. The results indicated that 1-hour obs-nudging had slightly better performance than the  
235 3-hour one. As a result, this study adopted 1-hour temporal frequency for observation nudging.

236 It should be noted that the default time interval for modified gridded analyses (i.e., the "metoa-  
237 em" files) have to match input analysis data in OBSGRID, which is 3 hours. However, the  
238 "OBS\_DOMAIN" output frequency is controlled by another namelist variable, which can be  
239 changed to hourly. This means that the OBSGRID output files, "metoa\_em" and  
240 "OBS\_DOMAIN", did not have the same time interval in our study.

241 In WRF, there were a few namelist variables controlling the frequency of grid nudging and  
242 observation nudging. These variables include: "interval\_seconds" for grid nudging files ("met-  
243 em"); "sgfdda\_interval\_m" for surface grid nudging files ("sgfdda"); and "auxinput11\_interval"  
244 for obs-nudging files ("OBS\_DOMAIN"). There is also "obs-ionf", which determines the  
245 nudging frequency relative to internal integration time-step.

246 One departure from the default OA setting in WRF was that the moisture OA was turned off with  
247 "obs\_nudge\_mois" set to 0. This was based on our past experiences since performing moisture  
248 OA sometimes trigger excessive artificial thunderstorms which disrupted model flow fields.

### 249 **2.2.2. Emission Processing**

250 For anthropogenic sources we utilized the National Emission Inventory of 2008 (NEI2008)  
251 generated by the USEPA. The mobile emissions were processed with EPA's Motor Vehicle  
252 Emission Simulator (MOVES). Using the Sparse Matrix Operator Kernel Emissions (SMOKE)  
253 Modeling System v3.1 the inventory was converted to gridded emission rates as well as to  
254 emission species as listed in the Carbon Bond 05 (CB05) chemical mechanism that is used in

255 CMAQ modeling. The biogenic emissions were estimated using the Biogenic Emissions  
256 Inventory System (BEIS) v 3.14. Although NEI2008 might have overestimated NO<sub>x</sub> emissions in  
257 Houston (e.g., Choi 2012; Czader et al. 2015) which could have impacted on ozone formation in  
258 the region, we used base NEI2008 without adjustment because the adjustment of the NO<sub>x</sub>  
259 emission also has large uncertainty. Pan et al. (2015) showed that the CMAQ ozone performance  
260 using NEI2008 appears reasonable.

### 261 **2.2.3. CMAQ Configurations**

262 The USEPA's CMAQ (Byun and Schere 2006) version 5.0.1 was adopted for this study,  
263 following the choice of several other Houston air quality modeling studies (e.g., Foley et al.  
264 2010; Czader et al. 2013, 2015; Choi 2014; Pan et al. 2015). CMAQ horizontal domains were  
265 slightly smaller than the WRF counterpart in order to avoid the discontinuity near the domain  
266 boundary. The domains were shown in Figure 2 as green and brown boxes. The chemical  
267 boundary conditions for all the species in the 4-km domain were derived from 12-km domain air  
268 quality forecasting results (<http://spock.geosc.uh.edu>). Vertically, CMAQ inherited the same  
269 layers from WRF without layer collapsing. Major CMAQ configurations were described in Table  
270 2. The texts in the parentheses were the values in the CMAQ build script.

271 Chemical processes were simulated with the available in CMAQ CB05 chemical mechanism  
272 with active chlorine chemistry, and updated toluene mechanism. For aerosol modeling, the fifth-  
273 generation CMAQ aerosol mechanism (AE5) with sea salt is selected. Cloud/aqueous chemistry  
274 is included. The total number of included species is 132, with 70 reactive gas-phase, 49 aerosol  
275 and 13 non-reactive species.

276

## 277 **3. Evaluation Metrics**

278 To assess model performance against observations, we computed a set of five statistics including  
279 Pearson correlation, index of agreement (IOA, Willmott 1981), mean bias (MB), root mean  
280 square error (RMSE), and Mean Absolute Error (MAE), similar to Li et al (2008). The goal is to  
281 have a comprehensive comparison between model and observation time series. These statistics  
282 have been frequently used for performance evaluation in modeling community.

283 The set of five statistics was divided into three groups:

284 1) Measuring the direct departure of model results from observation, in measurement units

- 285 • Mean Bias (MB)
- 286 • Mean Absolute Error (MAE)
- 287 • Root Mean Square Error (RMSE)

288 2) Measuring how close the model values follow changes in the observations, unitless

- 289 • Correlation

290 3) A composite performance index, index of agreement (IOA or d), unitless

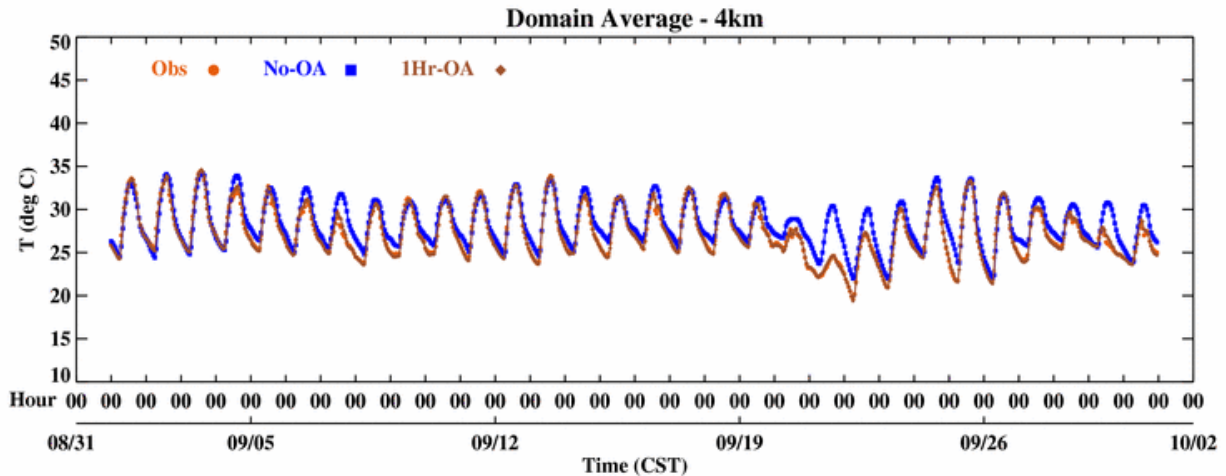
291 IOA is considered a better performance index than correlation as it takes into account the  
292 difference in the means and standard deviation. For example, when correlations are similar,  
293 lower model biases would yield higher IOA values.

294 Additionally, the mean and the standard deviation (Std. Dev.) of model values and observations  
295 were included as a reference.

296

#### 297 **4. General Meteorological and Ozone Conditions in September 2013**

298 The weather during the September 2013 simulation period was relatively dry with mostly  
299 southerly, easterly or southeasterly winds. From 5 to 19 September, there was a lack of influence  
300 of strong synoptic weather systems. Shifting wind patterns were observed during the period: light  
301 northeasterly in the early morning gradually turned clockwise to southeasterly in the afternoon  
302 and evening hours. In this period, winds shifted from southeast to near east and there were more  
303 clouds after 10 September. The only cold front arrived on the early morning of 21 September.  
304 Figure 3 shows the regional average temperatures for the period and it can be seen that 21  
305 September has the lowest daily high temperature. The influences of the cold air intrusion lasted  
306 till early 25 September. Winds turned into southerly in the afternoon of the 25<sup>th</sup> and warming  
307 continued in the next few days.



308

309 **Figure 3.** Regional hourly temperature averaged over all available hourly CAMS observations,  
 310 two model cases also included for September of 2013.

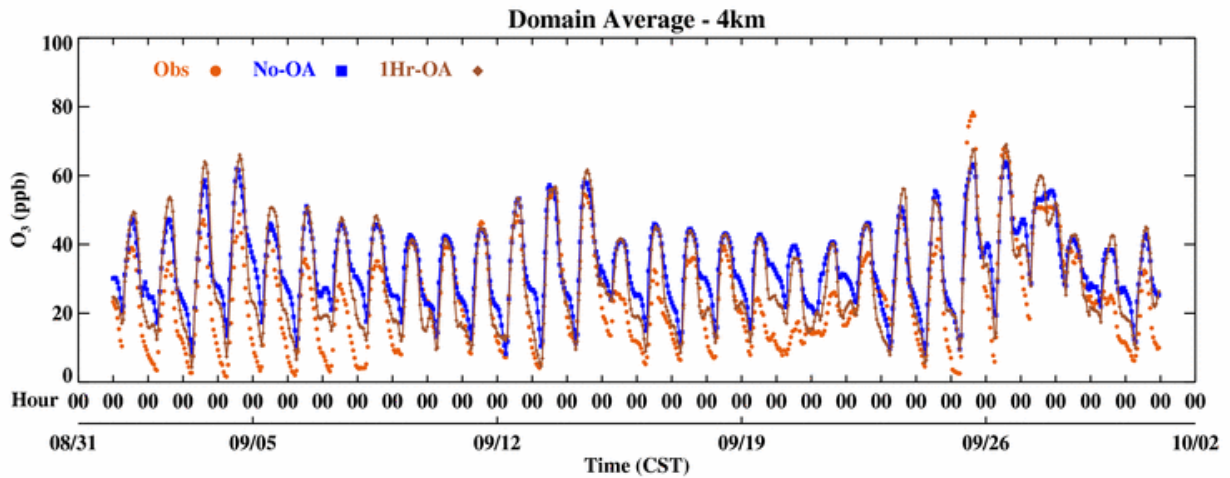
311 Rain events occurred on 09/02, 09/10, 09/16, 09/19 to 09/21 and 09/28 to 09/30. None of them  
 312 was heavy. The 09/20 and 09/21 events consisted of widespread light to medium showers.  
 313 Besides the above-mentioned dates, there were a few other days with sporadic drizzles.

314 A majority of the days between 09/01 and 09/20 were mostly sunny to mostly cloudy. The  
 315 periods from 09/08 to 09/10 and 09/18 to 09/20 had more clouds than other days. The period  
 316 from 09/21 to 09/30 was influenced by a cold front passage. The days between 09/22 and 09/24  
 317 were sunny and cool. Then the surface wind reversed direction during mid 09/25 and brought  
 318 clouds back from 09/26 to 09/30.

319 In SETX, high ozone events in fall season were typically associated with a passage of cold front  
 320 (e.g., Rappenglueck et al. 2008). The only ozone event with hourly surface ozone exceeding 120  
 321 ppb (parts per billion) in September, which occurred on the 25<sup>th</sup>, fell in this category.

322 Figure 4 shows the hourly regional averaged ozone. On most days, the observed high averaged  
 323 ozone are below 70 ppb. Since the winds after dawn consistently pushed the precursors from the  
 324 industrial area to the southwest of the city, the wind pattern did not favor the local ozone  
 325 production. The daytime winds also contained a persistent easterly component which moved the  
 326 pollutants away from the Houston metropolitan area. In the first 10-day period, less background  
 327 ozone originating from the Gulf of Mexico contributed to the low-ozone days. With overcast

328 skies on the 19<sup>th</sup> and the 20<sup>th</sup>, hourly high ozone values dipped below 30 ppb. The two highest  
329 ozone days, characterized by post-frontal ozone events, were the 25<sup>th</sup> and the 26<sup>th</sup>.



330

331 **Figure 4.** The hourly regional averaged ozone for the two cases (No-OA and 1hr-OA) at the  
332 stations which include observation surface O<sub>3</sub> over the 4km domain for September of 2013.

333

## 334 5. Evaluation of Simulation Results

335 To evaluate the WRF simulation, we calculated statistics for surface temperature and winds in  
336 the 4-km domain. For PBL heights, we chose to plot out the time-series for the one site we had  
337 observations due to significant amount of missing data (data coverage is about 50%). For CMAQ  
338 evaluation, we calculated the surface ozone statistics for the whole month. Also, we plotted  
339 vertical ozone profile and calculated biases for ozone aloft on 09/25.

### 340 5.1. Meteorology

#### 341 5.1.1. Temperature

342 The comparison of regional average hourly temperature for the analyzed time period is shown in  
343 Figure 3. The regional averaged temperature was calculated by averaging the hourly temperature  
344 from ~60 CAMS sites in the 4-km model domain. Overall the simulated averaged temperatures  
345 tracked the in-situ data well. It was also evident that the “1Hr-OA” case matched better with the

346 observations in several time periods, especially for September 20-23. The base case temperature  
347 is too high.

348 The statistics of hourly surface temperature are presented in Table 3. With higher IOA and lower  
349 mean biases (MB), the “1Hr-OA” case was clearly better than the base case “No-OA”. The IOA  
350 of “1Hr-OA” was about 9% higher than the base case.

### 351 **5.1.2. Winds**

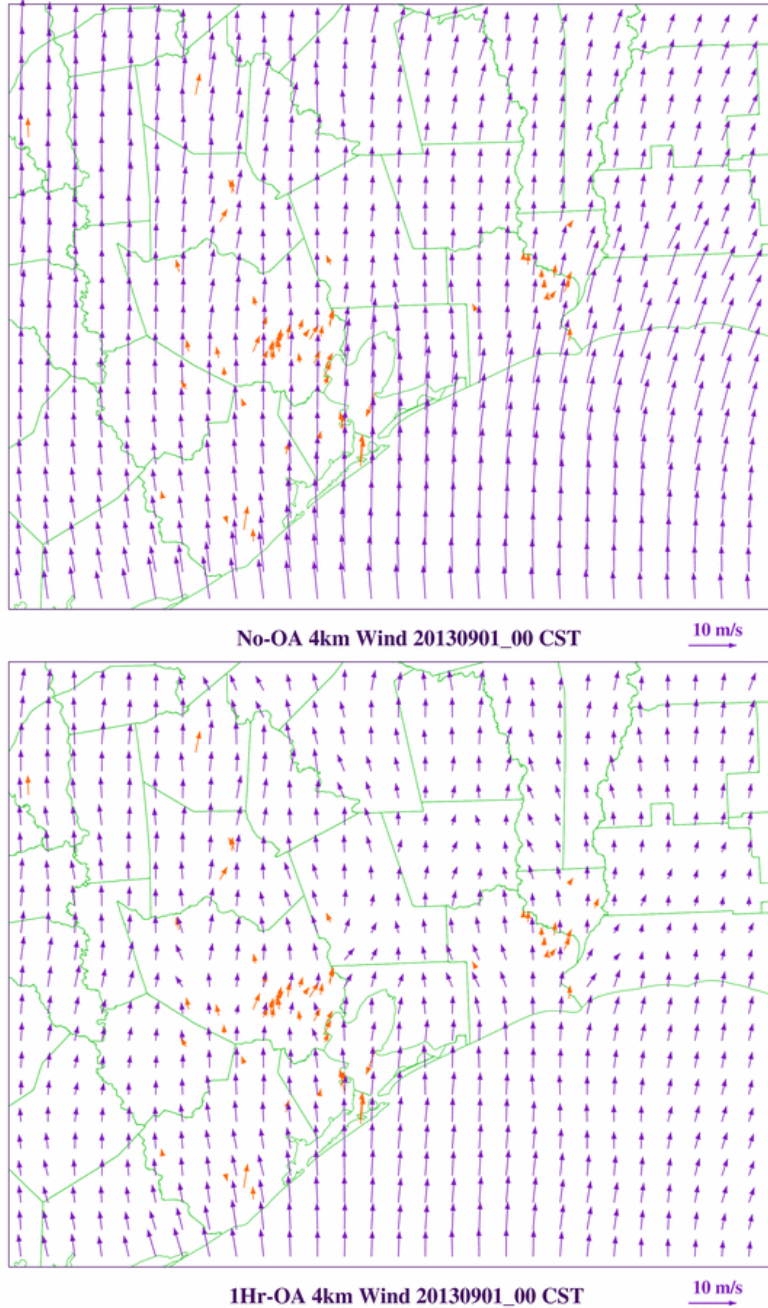
352 Wind fields are known to significantly affect chemistry (e.g., Banta et al. 2005, 2011; Darby  
353 2005). In ozone chemistry, winds affect the accumulation of precursors and hence the resulting  
354 ozone production. Winds are also responsible for dispersing high ozone and bringing background  
355 ozone. In HGB, prevailing southerly to southeasterly winds in the summer time significantly  
356 lowered the ozone level in the metro area. Therefore, high ozone events usually occur when such  
357 wind pattern changes. Cold front intrusion, coming as early as late August, blows pollutants to  
358 the south. As a result, an area of high ozone develops in the Gulf. A few days later, cold fronts  
359 weaken and reversing winds bring ozone back. High ozone also occurs during intra-day pollutant  
360 recirculation events when pollutants previously blown away from industrial zone are brought  
361 back by reversing winds. The high ozone event in the HSC area on 09/25 was likely due to a  
362 combination of local recirculation caused by onset of the bay breeze and increased background  
363 ozone brought in by transport.

364 Due to the land-water thermal contrast and the different size of the Galveston Bay and the Gulf  
365 of Mexico, the western shore of the Galveston Bay often experiences a successive onset of bay  
366 breeze and sea breeze in the summer. The bay breeze is typically a weaker easterly while sea  
367 breeze is a stronger southeasterly. Sea breeze usually comes one to a few hours later after the bay  
368 breeze. The bay breeze and the subsequent sea breeze phenomena in Houston were described by  
369 Banta et al. (2005).

370 The statistics of zonal (U-WIND) and meridional (V-WIND) wind components are listed in  
371 Table 3. The purpose of choosing U and V over wind speed and direction is to avoid the  
372 anomalies in the wind direction statistics. For example, although wind direction of 5 and 355  
373 degrees are close, the statistics suggest that they are distinctively different.

374 For both U and V components of wind, "1Hr-OA" had higher correlation and IOA than "No-  
375 OA". The model performance on U and V are similar, with the correlation in a range of 0.76 to  
376 0.81 for all the cases. As a reference, the performance of the OA case ("M1") in Ngan et al.  
377 (2012) is very close to that in this study, with a correlation of 0.75 for U and 0.82 for V. In terms  
378 of IOA, the OA case had a larger lead over the base case, ahead by 5-6% in U and 10-11% in V  
379 over the base case. This can be explained by the much reduced wind biases in the OA case.

380 The base case had consistently stronger winds, especially the southerly component, than the  
381 observation. This was reflected in the mean bias "MB", as well as the model mean "M\_M".  
382 Winds were reduced significantly after OA was performed. Interestingly, the high southerly bias  
383 in "No-OA" turned slightly negative after OA. Winds originating from the Gulf were also  
384 stronger in base case, which played a role in raising the ozone level comparing to the sensitivity  
385 case. Figure 5 illustrated the slowing down of southerly winds after observation nudging. As a  
386 result, winds matched better to the observations.



387

388 **Figure 5.** Model and observed winds at 09/01\_00 CST: No-OA (top) and 1Hr-OA (bottom).  
 389 Model winds are blue arrows and the observations are orange arrows. Stronger southerly winds,  
 390 especially along coastal region, were reduced in the OA case.

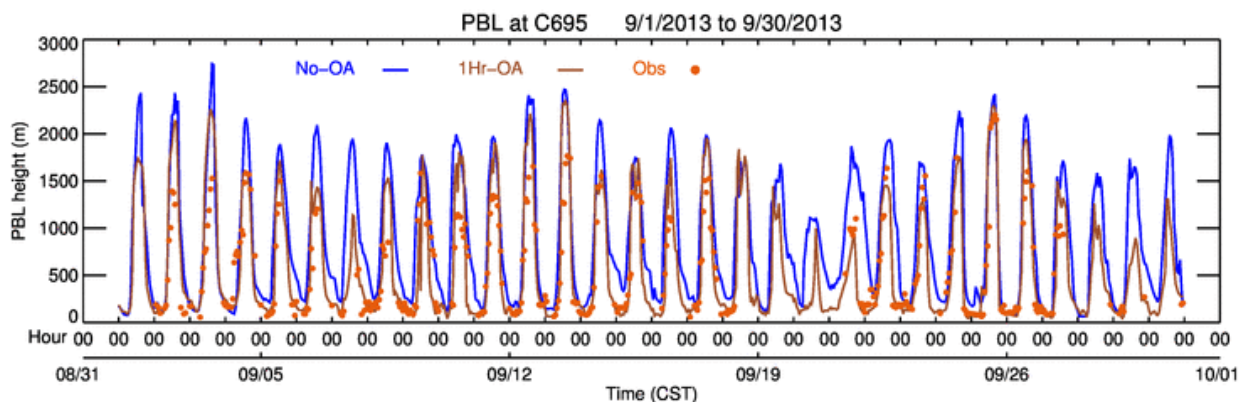
### 391 **5.1.3. PBL height**

392 Atmospheric pollutants are largely confined in the PBL as most of the emissions sources are  
 393 close to the ground level. PBL plays a critical role in mixing and spreading the pollutants.

394 Haman et al. (2014) studied the relationship between ozone level and PBL height at a Houston  
395 CAMS site and found that nighttime and early morning PBL heights were consistently lower on  
396 high ozone days than on low ozone days. Czader et al. (2013) pointed out that the model  
397 underprediction of PBL during nighttime may have caused the CO overprediction at the same  
398 site. CO is a good proxy for understanding model's transport since it has low reactivity and a  
399 relatively long life time in the troposphere.

400 Cuchiara et al. (2014) conducted four WRF/Chem sensitivity tests on the PBL schemes over  
401 southeast Texas. While no preferred PBL scheme was identified for WRF simulations, the  
402 Yonsei University (YSU) scheme outperformed others in ozone prediction. As a note, YSU  
403 scheme is used in this study.

404 The PBL height data were taken at an urban site very close to CAMS site C695, located on  
405 University of Houston campus. A study by Haman et al. (2012) showed that Houston's daily  
406 maximum PBL height reached its highest values of slightly over 2000 m in August. In  
407 September, typical daily maximum PBL height was 1500 m at 15 CST while daily minimum was  
408 just below 200 m between 00 CST and 06 CST. The comparison of observed and model PBL  
409 height is shown at Figure 6. The model tended to overpredict the daily maximum and obs-  
410 nudging helped to reduce the overpredictions. For the daily minimum PBL height, "No-OA"  
411 case had slightly high biases while the OA case matched quite well with observations. The  
412 observed minimum PBL height was lower than that reported by Haman et al. (2012), likely due  
413 to the cloudy condition in September 2013. There was no apparent explanation on the reduced  
414 daytime PBL biases in the OA case than the base case, but it is likely the results of improved  
415 winds and temperatures in PBL.



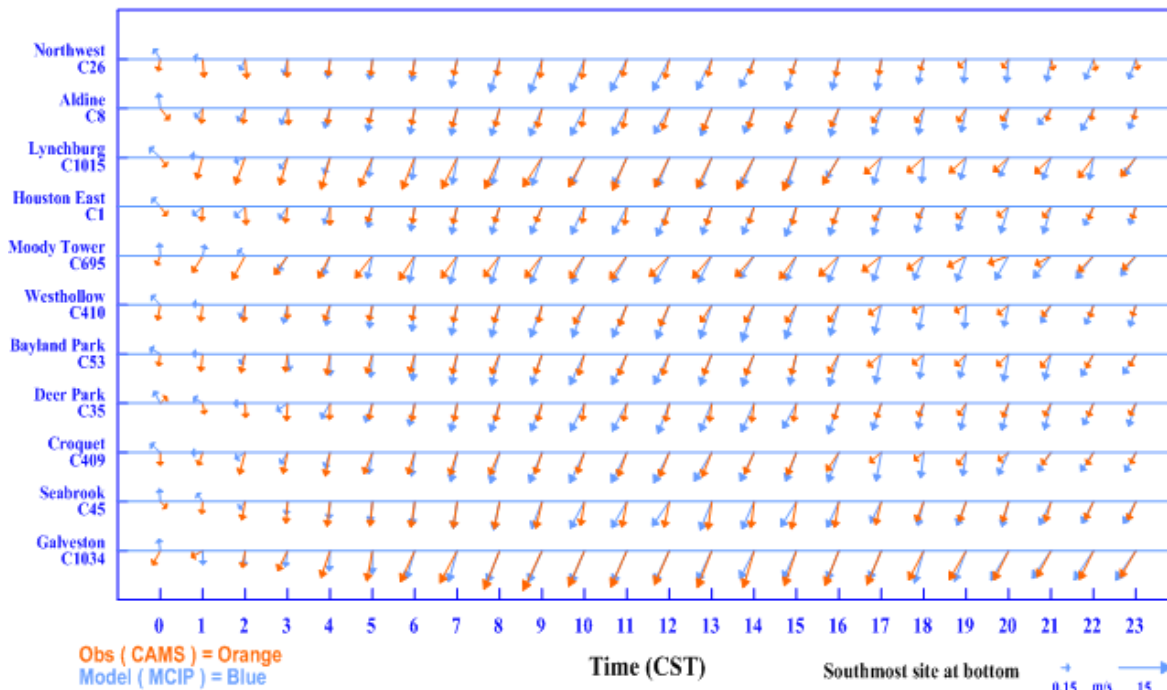
417 **Figure 6.** Planetary Boundary Layer (PBL) height time series at CAMS C695 for September  
418 2013.

#### 419 **5.1.4. Cold Front Passage**

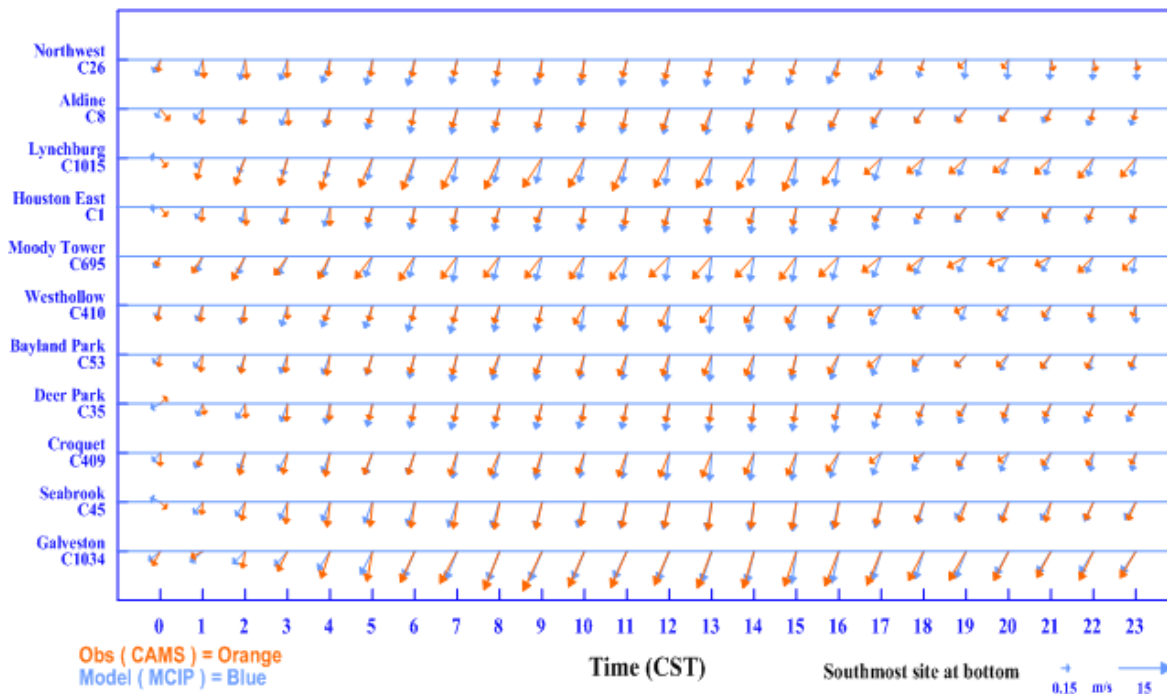
420 The surface winds on 09/20 were overwhelmingly southerly in the region and reversed on 21  
421 September due to the arrival of a cold front. The hour-by-hour wind shifts for 11 sites in HGB on  
422 21 September are plotted in Figure 7. The sites are sorted by latitude with the southernmost site,  
423 Galveston C1034, located at the bottom row. There was only one site, Deer Park C35, showing  
424 weak southerly at 00 CST while all the others had mostly weak northerly. Starting from 01 CST,  
425 winds in the entire HGB area turned northerly to northeasterly and continued gaining strength in  
426 the next few hours, indicating cold air had taken over the region.

427 Both cases performed reasonably well on 09/21 and the timing of wind shift was captured quite  
428 accurately although “No-OA” lagged about an hour. The winds turned weak northerly at 00 CST  
429 for most sites and “No-OA” still showed all southerly. Besides the timing, the northeasterly  
430 winds in “No-OA” case sometimes were too strong and obs-nudging helped moderate the winds.  
431 The reduced V-wind bias in “1Hr-OA” was also evident in wind statistics on 21 September. The  
432 performance of the OA case during cold front passage was consistent with our past simulations.

20130921: Houston Wind - No-OA



20130921: Houston Wind - 1Hr-OA



433

434 **Figure 7.** Hourly model (blue) and CAMS (orange) winds at 11 sites on 21 September: No-OA  
 435 (top) and 1hr-OA (bottom). The 1hr-OA case is better in 00 CST to 02 CST and 17 CST to 20  
 436 CST.

## 437 5.2. Ozone

### 438 5.2.1. Regional Average Hourly Ozone

439 Figure 4 showed the regional average hourly ozone, which was defined similarly to the averaged  
440 temperature. Overall observed ozone level was low and model did reasonably well on the timing  
441 of intra-day variations, though both cases tend to overpredict the daily highs and daily lows,  
442 especially in the first 8 days and between 15 and 21 September. An obvious departure is the 25<sup>th</sup>  
443 – both cases missed the daily high. During the model high bias period, the OA case usually did  
444 better in reaching the daily low although it overpredicted the high a bit more than the base case.  
445 The night time biases were reduced likely because the lower southerly winds in the OA case  
446 transported less ozone from the Gulf to the land.

447 We found that model had higher ozone concentration in the Gulf than the actual during the study  
448 period. In two time periods: 2<sup>nd</sup> – 4<sup>th</sup> and 7<sup>th</sup>-8<sup>th</sup> of September, the incoming ozone from the Gulf  
449 is markedly lower. Since the model ozone had fixed boundary values, the model was unable to  
450 capture the daily ozone variation at the boundary. The model has the highest biases during 19<sup>th</sup> -  
451 20<sup>th</sup> likely due to overcast skies and the problems in model's cloud fields and high background  
452 ozone values. Despite overprediction, the biases in OA case are notably lower during the nights  
453 of 19<sup>th</sup> and 20<sup>th</sup>. A future study to upgrade the accuracy of cloud fraction using remote sensing  
454 data (e.g., MODIS) should be helpful in explaining the biases.

455 There were a few days with elevated ozone due to post-front meteorology conditions. The only  
456 exceedance happened on 09/25, which was likely caused by meteorological events in Houston  
457 and the Galveston Bay. The overall ozone on 26 September was higher after southerly winds  
458 transported back the ozone from the Gulf, raising the ozone level in the entire region. A more  
459 detailed analysis of model predictions on 09/25 and 09/26 will be presented in following  
460 subsection of 5.2.3.

### 461 5.2.2. Performance Statistics

462 The ozone statistics were displayed in Table 4. Both cases had very close correlation of 0.72 and  
463 0.73. However, the mean biases in the OA case were lower by 3.2 ppb, which helped raise the

464 IOA from 0.78 to 0.83. The model standard deviation increased in the OA case and matched  
465 better with observation. The improvement in IOA was slightly less in temperature and winds.

### 466 **5.2.3. High ozone episode after the passage of a front**

467 In SETX, high ozone events during the fall season usually occurred after the passage of a cold  
468 front (e.g., Rappenglück et al. 2008; Ngan and Byun, 2011; Ngan et al. 2012, Haman et al.  
469 2014). Two factors may have contributed to the post-front ozone events: 1) following a cold spell  
470 winds reverse direction and subsequent light winds and sunny skies create an ideal condition for  
471 ozone production and accumulation 2) wind reversal transports back the pollutants that were  
472 blown into the Gulf previously, a phenomenon commonly known as recirculation.

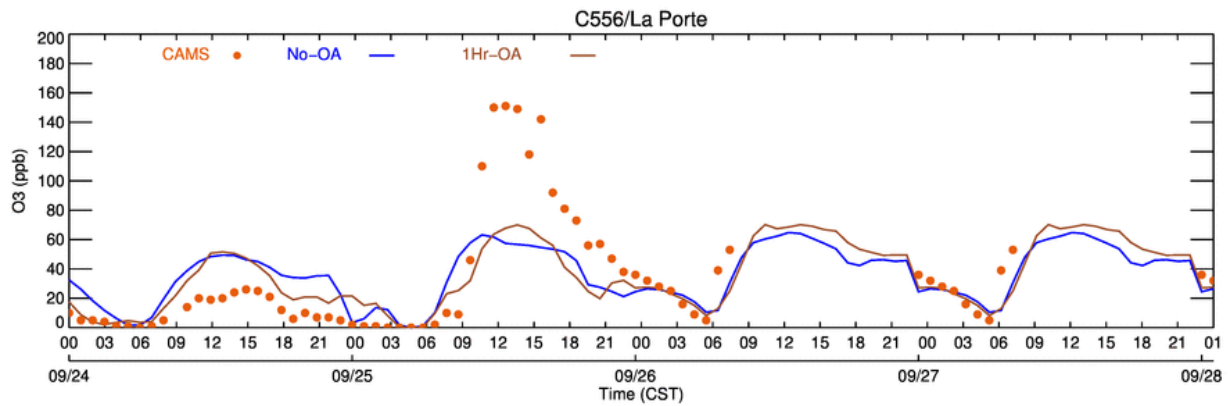
473 During the DISCOVER-AQ period, the two days with highest ozone were 25 September and the  
474 day 26 September (Figure 4), but the two days exhibited different patterns. The 1-hour maximum  
475 ozone on the 25<sup>th</sup> was localized and higher by about 40 ppb than the 26<sup>th</sup>. In addition to  
476 heightened background ozone on the 25<sup>th</sup>, the major contributor was the production resulting  
477 from favorable weather conditions: sunny, overall light winds and shifting winds over the  
478 industrial area. The light morning land breeze carried pollutants from ship channel area to the  
479 Galveston Bay. As the day warmed up, bay breeze started to develop and carry pollutants back to  
480 the land. This localized circulation was first described by Banta et al. (2005). Ngan et al. (2012)  
481 reported the same phenomenon in their Texas Air Quality Study-II 2006 study. The 26<sup>th</sup> is  
482 characterized by elevated background ozone from morning to late night.

483 Figure 8 shows the ozone time series of La Porte (C556), located in HSC area (Figure 1). In  
484 September, the highest hourly ozone of 151 ppb occurred at C556 at 13 CST of 25 September.  
485 From 9 CST to 12 CST, ozone rose from 10 ppb to 150 ppb. Such large increase in ozone was  
486 the result of chemical production under favorable meteorological condition in an area with  
487 accumulated precursors. Figures 9 and 10 depict the wind and ozone concentrations at 08 CST  
488 and 13 CST.

489 From the wind plots of Figure 9, we can see that the winds at 8 CST were light northerly for sites  
490 located on the north side while winds were mostly westerly for the sites in the middle and south.  
491 The base case winds were all northerly while OA case had northwest winds for north side and  
492 west winds for the middle and south. The winds in OA case were much more realistic. The 9

493 CST winds were similar to those of 8 CST. As a result, the ozone statistics in Table 5 showed  
494 that the OA case had much better correlation and IOA than the base case during 8-9 CST. This  
495 example demonstrated OA's ability to correct erroneous winds. However, later events showed  
496 OA may not always be able to perform consistently.

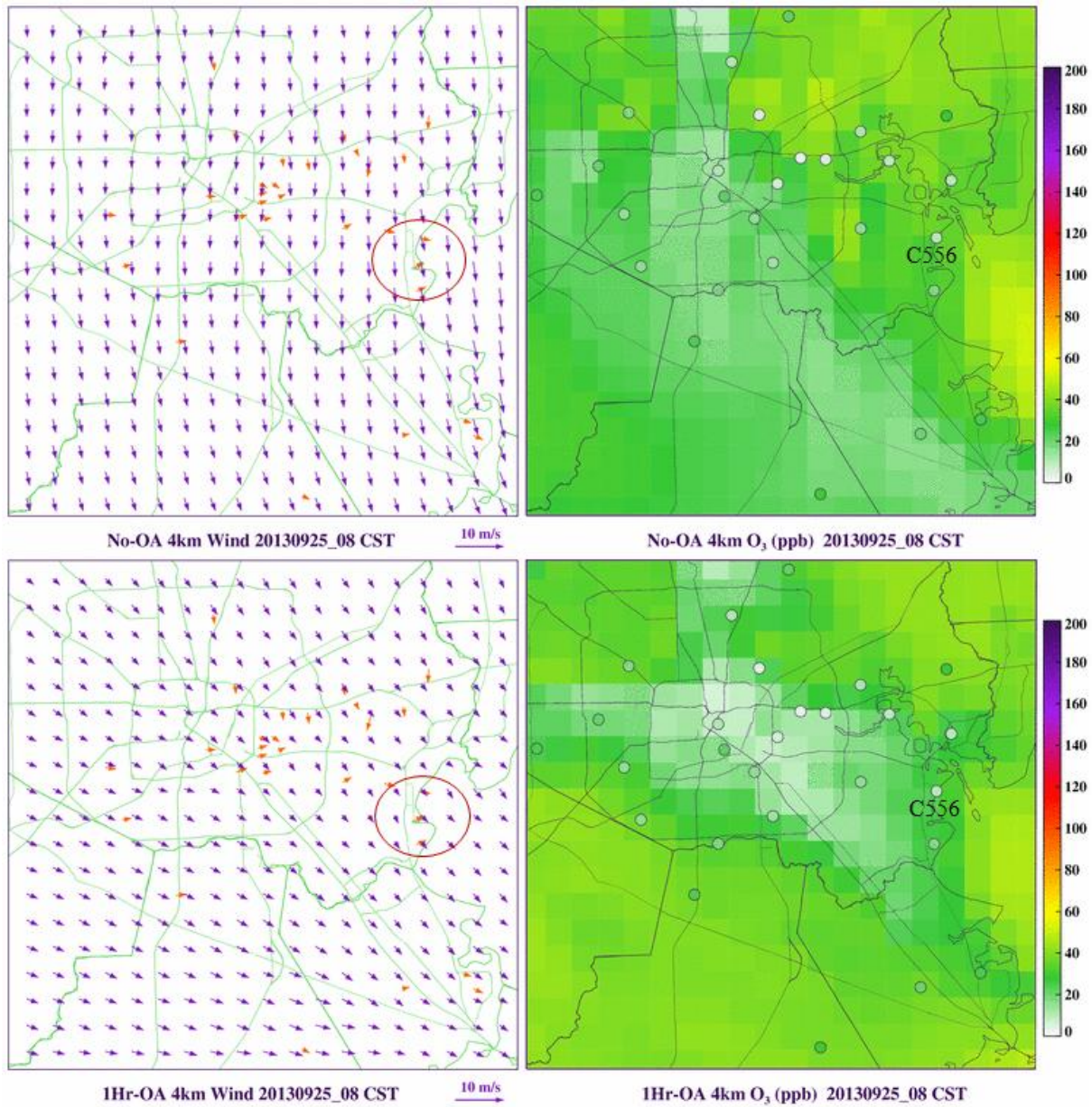
497 The bay breeze started to develop at 10 CST near C556. The early onset was likely to be related  
498 to the warming up the previous afternoon on 09/24 (Figure 3). At 10 CST most other sites to the  
499 west of HSC experienced light northwest winds while winds at HSC were from northeast.  
500 Combined with the easterly bay breeze, a convergence zone was formed just below C556, where  
501 emissions from the HSC area stalled and accumulated. At 13 CST, the whole region had light  
502 winds and the bay breeze was well developed. The highest ozone indeed appeared in C556 and  
503 its vicinity. The rapid increase of ozone concentration for C556 between 9-13 CST is shown in  
504 Figure 8.



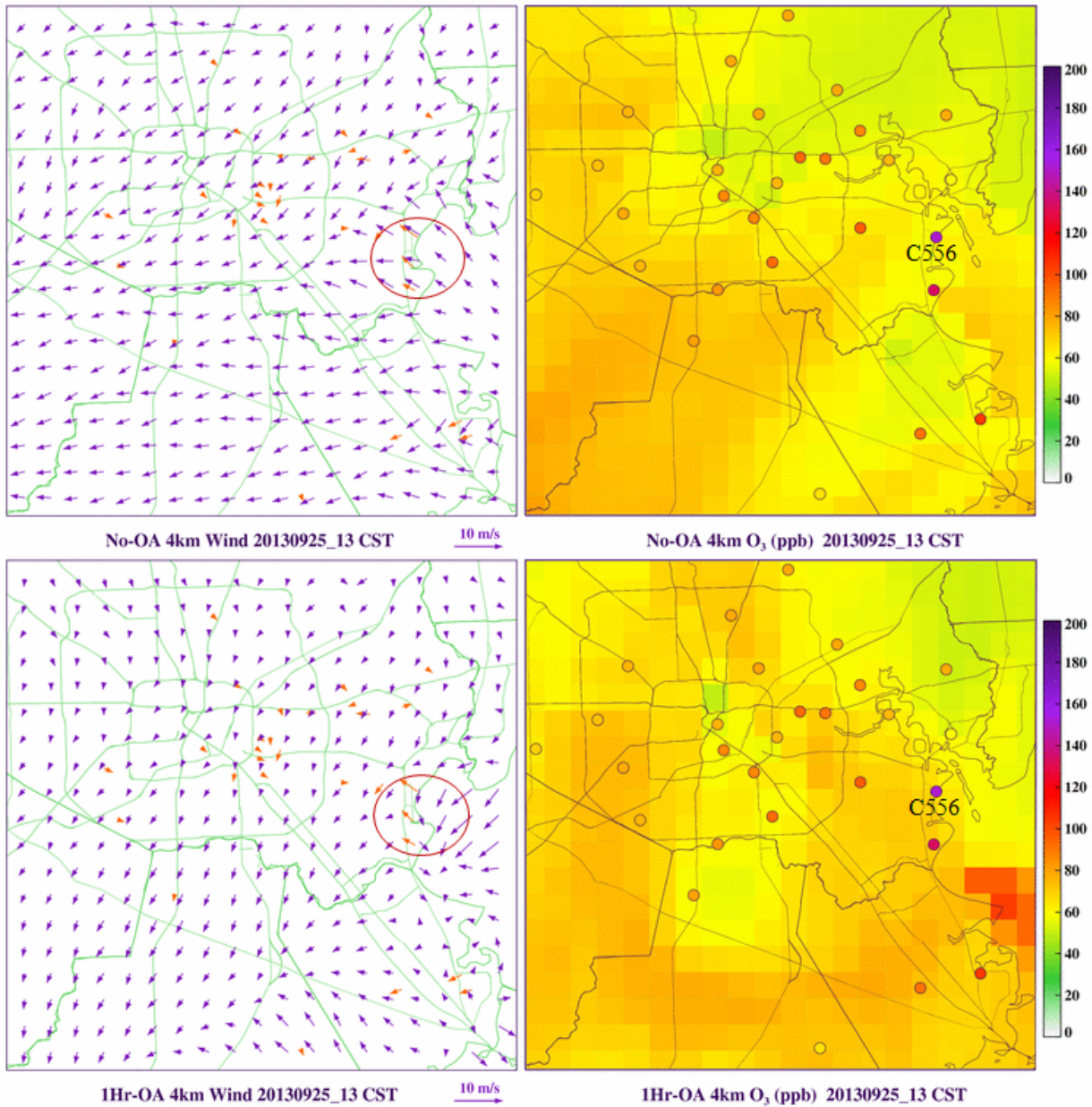
505  
506 **Figure 8.** Ozone time series of La Porte (C556) between 09/24\_00 to 09/28\_00 CST of 2013.

507 It is important to note that both modeled cases missed the wind shifts in the HSC area, and the  
508 resulted convergence zone near C556. This could explain the model's inability to recreate the  
509 sharp ozone increase at C556. Figure 9 shows that the ozone level around HSC area is quite low  
510 (~10 ppb) at 08 CST. A further examination showed that while both model cases missed the  
511 wind shift and convergence, though the patterns were different. The base case had flawed winds  
512 for most of the morning: instead of a weak westerly, it had stronger northwesterly to northerly.  
513 By 08 CST, winds were almost uniformly northerly in the base case while they were weak west-  
514 northwesterly in the OA case (Figure 9). The oval in Figure 9's top-left panel shows the

515 mismatch of winds around C556 in the base case. As a result, the  $\text{NO}_x$  produced in the city was  
516 carried further to the southeast in the model in the base case. Until 13 CST, base case winds did  
517 not shift directions by much. The OA case got the early hour weak northwesterly right, but  
518 missed the bay breeze onset between 10 and 13 CST (oval in Figure 10). The OA case could not  
519 reproduce the small-scale wind reversal near C556, suggesting there is a limitation in current  
520 WRF OA's capability. On the other hand, the OA case did improve the spatial ozone pattern, as  
521 the high ozone area was closer to HSC after OA (Figure 10).



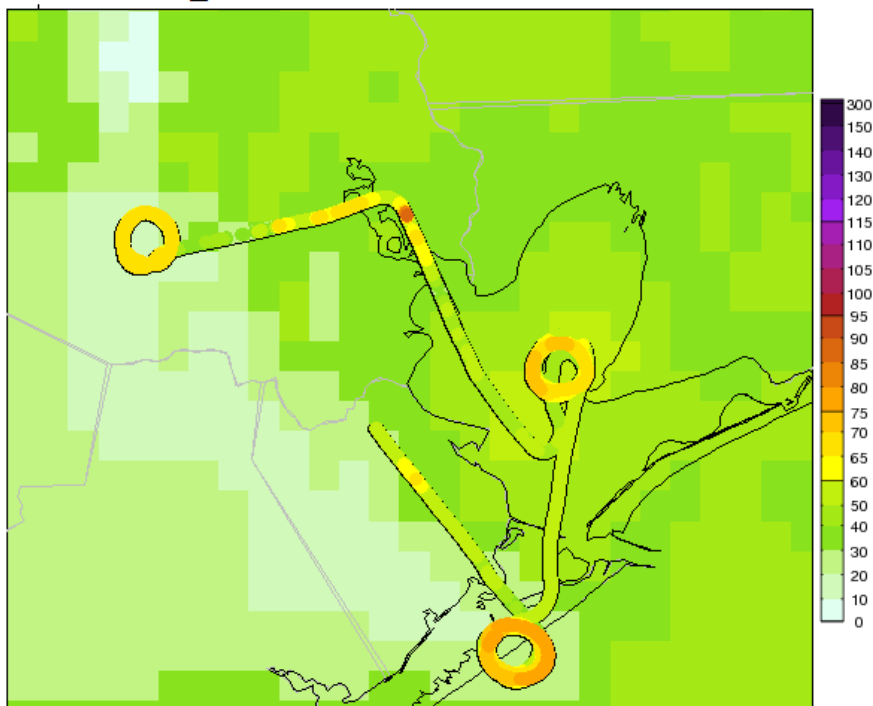
523 **Figure 9.** Zoom-in ozone concentrations (right) and wind plots (left) at 13 CST 25 September  
 524 for “No-OA” (top) and “1Hr-OA” (bottom). Ozone observation is in small circle; wind  
 525 observation is indicated by an orange arrow. La Porte site C556 is labeled. The value range of  
 526 right-side colour scale is 0 to 200 ppb. Higher value than 200 ppb has the same colour as 200  
 527 ppb.



528  
 529 **Figure 10.** Zoom-in ozone concentrations (right) and wind plots (left) at 13 CST 25 September  
 530 for “No-OA” (top) and “1Hr-OA” (bottom). Ozone observation is in small circle; wind  
 531 observation is indicated by an orange arrow. Bay breeze is shown in the orange oval.  
 532

533 The ozone measurements from aircraft P3-B provided a more complete picture for 09/25's ozone  
534 evolution. During the day, P-3B flew around the industrial area, Galveston Bay, and Galveston  
535 Island for about 9 hours. Figures 11 and 12 showed ozone concentrations along aircraft tracks at  
536 08 and 13 CST, with surface layer ozone from the "No-OA" case as background. The  
537 background was only intended as a reference. At 08 CST, ozone level of 60-80 ppb aloft was  
538 already observed at three locations (three loops in Fig.11): Galveston Island, Smith Point and  
539 inner city. Another high of ~90 ppb could be seen above the HSC area. Ozonesonde observations  
540 over HGB showed the ozone aloft were normally ~40-50 ppb (e. g., Li and Rappengluck 2014).  
541 The higher-than normal ozone aloft suggested a post-front ozone recirculation condition. Such  
542 high ozone aloft might raise surface ozone level as a growing PBL downwardly mixed the air  
543 aloft with near surface air. At 13 CST, high ozone over 100 ppb was observed at multiple  
544 locations. The highest ozone aloft, ~ 160 ppb, occurred southwest of Smith Point in the  
545 Galveston Bay. Such level of ozone increase was likely the result of active production in the  
546 industrial zone and around Galveston Bay.

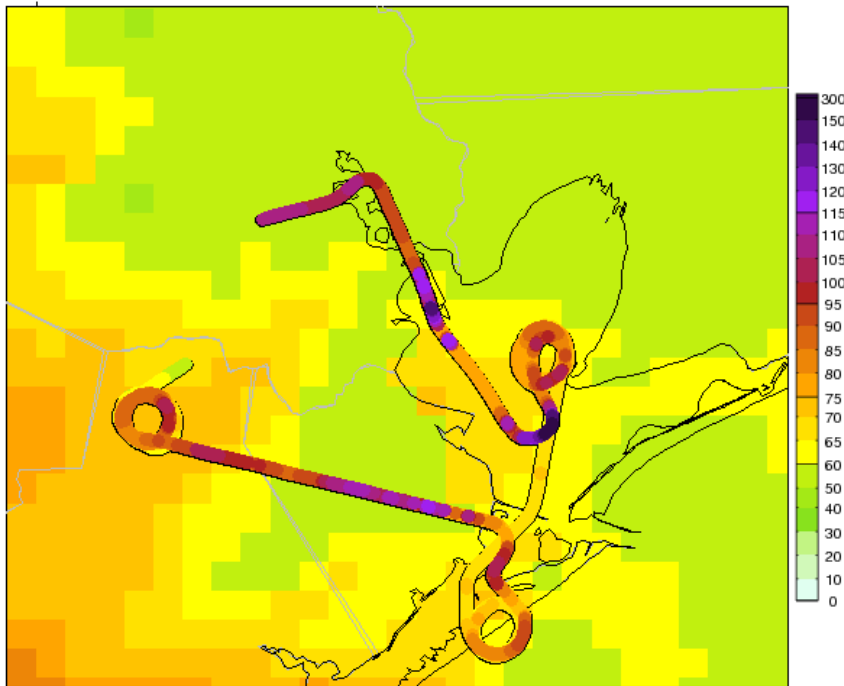
2013-09-25\_08 CST P3B Ozone with No-OA Surface



547

548 **Figure 11.** Ozone along aircraft tracks at 08 CST of September 25th, overlaid upon model No-  
549 OA surface ozone.

2013-09-25\_13 CST P3B Ozone with No-OA Surface

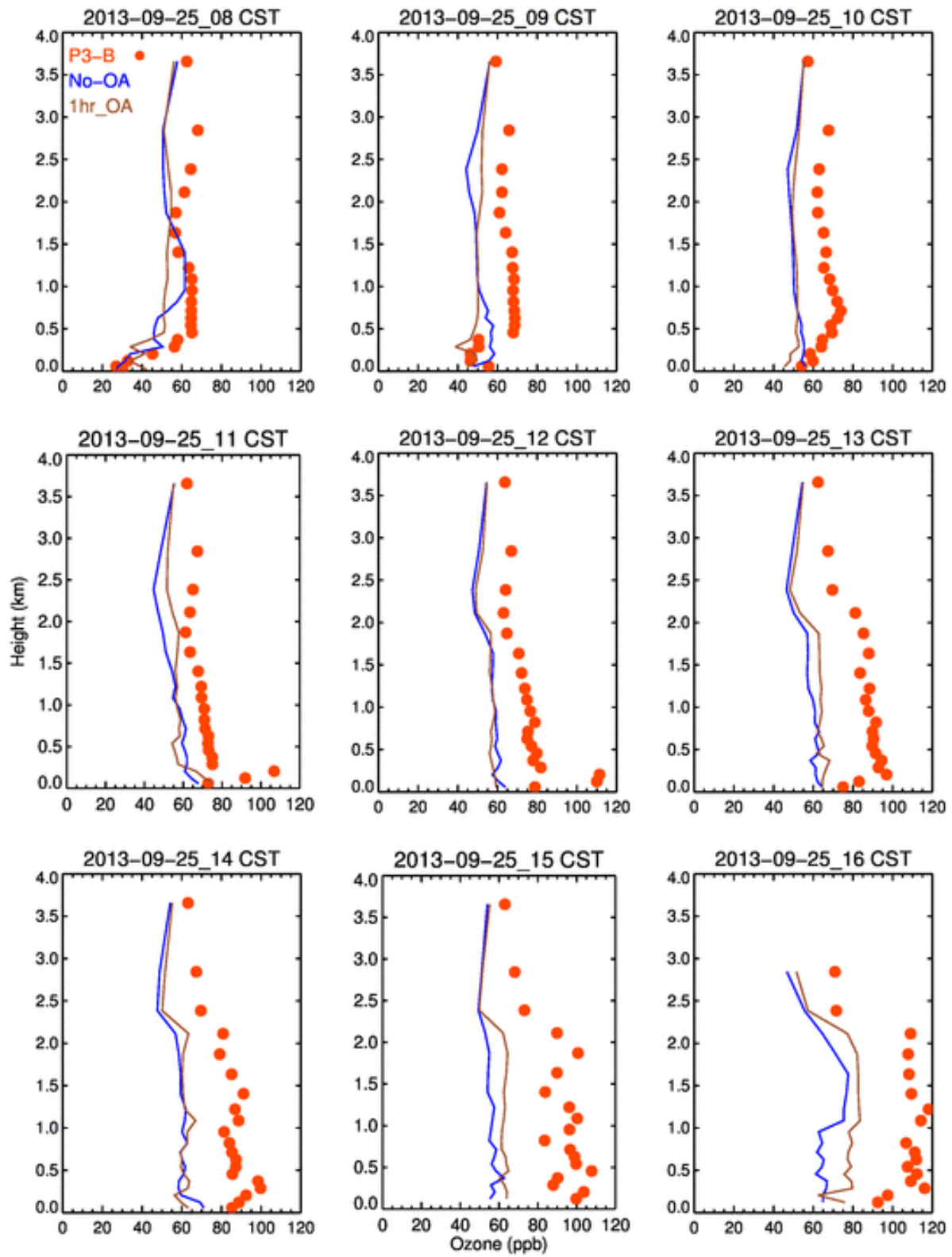


550

551 **Figure 12.** Ozone along aircraft tracks at 09/25\_13 CST of September 25th, overlaid upon model  
552 “No-OA” surface ozone. Plumes can be seen as dark purple circles in Galveston Bay.

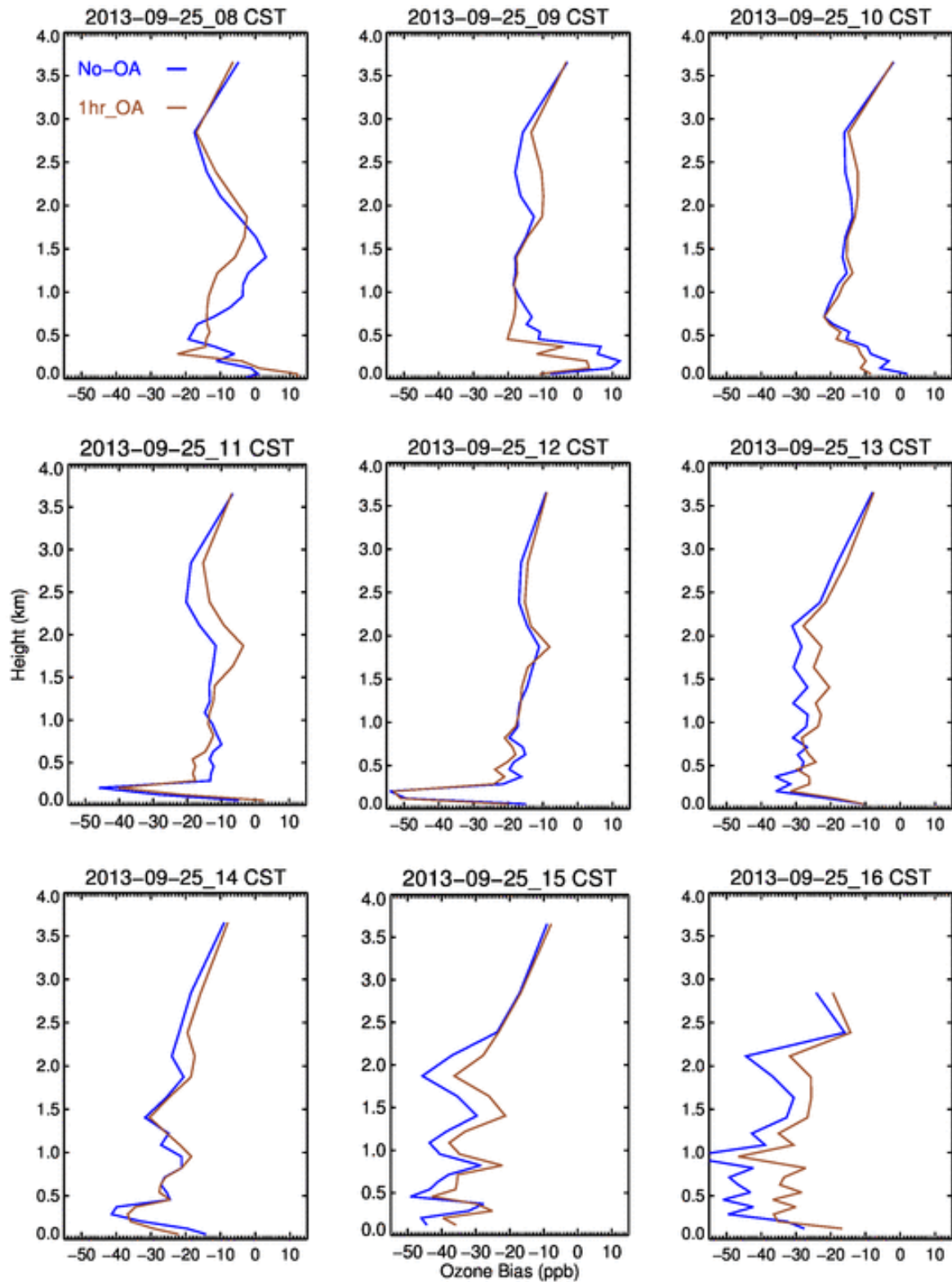
553 Figure 13 shows hourly ozone vertical profiles from 08 CST to 16 CST of September 25<sup>th</sup>, with  
554 ozone being displayed on the x-axis and height on the y-axis. The observed ozone was averaged  
555 over multiple measurements in the same model cell, such that they could be properly compared  
556 to model values. Then both model and observed ozone values was averaged over all the grid  
557 cells in the same model layer, such that one dot represents the average ozone of all the cells in  
558 the same layer. The 08 and 09 CST profiles showed there was a high ozone layer with average  
559 ozone of ~65 ppb, stretching from 450 m to 1200 m height. In comparison, all model runs had  
560 lower ozone in this layer. The model biases, as shown in Figure 14, were about -10 ppb at 08  
561 CST and grew to -20 ppb at 09 CST. The large discrepancy between low surface ozone and  
562 ozone aloft was unusual and may be explained by the arrival of high ozone air mass aloft. The  
563 observed ozone rose continuously in following hours yet model simulated ozone stagnated  
564 around 60 ppb from surface up to 2000 m until 15 CST. At 16 CST, the ozone of OA case in 0-1  
565 km layer rose 20 ppb over previous hours yet the base case ozone increased only a few ppb.  
566 Although different in magnitude, ozone aloft had a few similar features to the surface ozone.

567 Firstly, the model missed the observed high ozone in the afternoon by a large margin. For  
568 example, the base case underpredicted 0-1 km level ozone by up to 50 ppb. The primary cause  
569 for the lower ozone production was likely model's wind fields as both model and observation  
570 had clear sky in industrial area and Galveston Bay. Secondly, nudging clearly helped reducing  
571 the ozone biases aloft. In most plots of Figure 14, the OA case had lower biases than the base  
572 case. The largest difference was at 16 CST, when nudging reduced biases from ~45 ppb to ~30  
573 ppb in the 300 – 1000 m layer.



574

575 **Figure 13.** Vertical ozone profiles from 09/25\_08 CST to 09/25\_16 CST of 2013 for two cases  
 576 of No-OA and 1Hr-OA compared with corresponding observations.



577

578 **Figure 14.** Model vertical ozone biases from 09/25\_08 CST to 09/25\_16 CST of 2013 for two  
 579 cases of No-OA and 1Hr-OA.

## 580 6. Conclusions and Discussions

581 In this study, we performed two Weather Research and Forecasting (WRF) and Community  
582 Multiscale Air Quality (CMAQ) model simulations to explore model sensitivity to observation  
583 nudging. In evaluating meteorological and ozone conditions, we found that obs-nudging  
584 improved the meteorology and ozone performance as shown in the index of agreement (IOA) of  
585 temperature, winds, and ozone. While the base case winds were overall well simulated, obs-  
586 nudging significantly reduced the high wind biases (especially the meridional wind) shown in the  
587 base case. For planetary boundary layer height, obs-nudging reduced high biases in both daily  
588 maximum and daily minimum values. In the end, the combined changes in meteorology lowered  
589 the ozone biases by about 3 ppb, a 35% reduction. There were short time periods (such as  
590 between 07 and 09 CST on 09/25) the base case model winds differ greatly from observation and  
591 obs-nudging significantly corrected the problems, leading to much better ozone simulation. It  
592 should be noted that the model ozone biases are also impacted by the emissions and model lateral  
593 boundary conditions.

594 While it is easy to understand the improvements in temperature and winds after obs-nudging was  
595 applied, it is more difficult to explain how other variables such as precipitation and clouds  
596 reacted to obs-nudging. The indirect impact of these meteorological variables on ozone was  
597 harder to assess. In our study, we did not evaluate clouds quantitatively as there were no  
598 digitized cloud fraction data available for our modeling domains. A preliminary analysis on  
599 convection showed that there were occasions in which model missed the convection or  
600 precipitation and there were other occasions in which model created artificial convection. The  
601 convection cells were usually visible as “star-burst” from surface wind vector plots – arrows  
602 going out to different directions from a center. However, the mismatch in convection appeared to  
603 be not a serious issue since only a few occurrences were observed in the month of September.

604 The only high ozone episode in the simulation period was related to the cold front passage. The  
605 small-scale winds and high ozone aloft on 09/25, likely contributed to the ozone exceedance in  
606 the area. It is also possible that unreported emission upset played a role. Since the maximum  
607 surface ozone at La Porte was much higher than the morning-time ozone aloft, the active local  
608 ozone production was likely the dominant factor. Analyses of ozone aloft on 09/25 showed while

609 there was high ozone aloft and large negative model biases, the OA case tended to have smaller  
610 biases, especially in late hours.

611 Small-scale meteorological events are frequently cited for their contributions to high ozone  
612 events. Model's capability in reproducing these events is critical in simulating such high ozone  
613 episodes. The base case did not recreate the 25 September small-scale events likely due to the  
614 complex winds and a lack of local information which can be used to steer model state closer to  
615 reality. On the other hand, the inability of the sensitivity case to replicate the local winds is likely  
616 a result of the imperfection of the nudging process pending further investigation. An ongoing  
617 study by the current authors suggests that errors in the meteorological fields from the default grid  
618 nudging files are important sources. Methods are being tested to improve the quality of grid  
619 nudging files. Early results showed that the bay breeze which caused the wind reversal around La  
620 Porte was well captured through improved grid nudging files. In addition, more observational  
621 data (e.g., more sites and higher data frequency) and more testing on the combination of nudging  
622 setting should help improve the obs-nudging performance. Also, the impact of obs-nudging on  
623 precipitation and clouds should be further investigated to understand their chain effect on  
624 chemistry.

## 625 **Acknowledgement**

626 The authors thank Texas Air Research Center (TARC) for its support through grant number  
627 413UHH0144A and Air Quality Research Program (AQRP) through 14-014, the DISCOVER-  
628 AQ team for the aircraft data, Vanessa Caicedo for LIDAR data, and the TCEQ CAMS site team  
629 for the in-situ ozone and meteorological data.

630 **References**

- 631 Banta, R. M., Senff, C. J., White, A. B., Trainer, M., McNider, R. T., Valente, R. J., Mayor, S.  
632 D., Alvarez, R. J., Hardesty, R. M., and Parrish, D.: Daytime buildup and nighttime transport of  
633 urban ozone in the boundary layer during a stagnation episode, *Journal of Geophysical Research:*  
634 *Atmospheres* (1984–2012), 103, 22519-22544, 1998.
- 635 Banta, R. M., Senff, C. J., Nielsen-Gammon, J., Darby, L. S., Ryerson, T. B., Alvarez, R. J.,  
636 Sandberg, S. R., Williams, E. J., and Trainer, M.: A bad air day in Houston, *Bulletin of the*  
637 *American Meteorological Society*, 86, 657+, 10.1175/bams-86-5-657, 2005.
- 638 Banta, R. M., Senff, C. J., Alvarez, R. J., Langford, A. O., Parrish, D. D., Trainer, M. K., Darby,  
639 L. S., Hardesty, R. M., Lambeth, B., Neuman, J. A., Angevine, W. M., Nielsen-Gammon, J.,  
640 Sandberg, S. P., and White, A. B.: Dependence of daily peak O<sub>3</sub> concentrations near Houston,  
641 Texas on environmental factors: Wind speed, temperature, and boundary-layer depth, *Atmos*  
642 *Environ*, 45, 162-173, 10.1016/j.atmosenv.2010.09.030, 2011.
- 643 Byun, D., and Schere, K. L.: Review of the governing equations, computational algorithms, and  
644 other components of the models-3 Community Multiscale Air Quality (CMAQ) modeling  
645 system, *Applied Mechanics Reviews*, 59, 51-77, 10.1115/1.2128636, 2006.
- 646 Byun, D., Ngan, F., Li, X., Lee, D., Kim, S.: “Analysis of Air Pollution Events in Summer 2006  
647 and Preparation of Model Input Data for the Assessment Study”, Grant No. 582-5-64594- FY07-  
648 02, Final Report: Evaluation of Retrospective MM5 and CMAQ Simulations of TexAQS-II  
649 Period with CAMS Measurements, Texas Commission on Environmental Quality, February,  
650 2008, 25 pp
- 651 Cheng, F.Y., and Byun, D. : Application of high resolution land use and land cover data for  
652 atmospheric modeling in the Houston-Galveston metropolitan area, Part I: Meteorological  
653 simulation results, *Atmos. Env.*, 42, 7795-7811, 10.1016/j.atmosenv.2008.04.055, 2008.
- 654 Cheung, V. T., and Wang, T.: Observational study of ozone pollution at a rural site in the  
655 Yangtze Delta of China, *Atmos. Env.*, 35, 4947-4958, 2001.

656 Choi, Y., Kim, H., Tong, D., and Lee, P.: Summertime weekly cycles of observed and modeled  
657 NO<sub>x</sub> and O<sub>3</sub> concentrations as a function of satellite-derived ozone production sensitivity and  
658 land use types over the Continental United States, *Atmos. Chem. Phys.*, 12, 6291-6307, 2012

659 Choi, Y.: The impact of satellite-adjusted NO<sub>x</sub> emissions on simulated NO<sub>x</sub> and O<sub>3</sub> discrepancies  
660 in the urban and outflow areas of the Pacific and Lower Middle US, *Atmos Chem Phys*, 14, 675-  
661 690, DOI 10.5194/acp-14-675-2014, 2014.

662 Choi, Y. and Souri, A.: Chemical condition and surface ozone in large cities of Texas during the  
663 last decade: observational evidence from OMI, CAMS, and Model Analysis, *Remote Sensing of*  
664 *Environment*, 168:90-101, DOI:10.1016/j.rse.2015.06.026, 2015

665 Cuchiara, G. C., Li, X., Carvalho, J., and Rappenglück, B.: Intercomparison of planetary  
666 boundary layer parameterization and its impacts on surface ozone concentration in the  
667 WRF/chem model for a case study in Houston, Texas, *Atmos Environ*, DOI  
668 10.1016/j.atmosenv.2014.07.013, 2014.

669 Czader, B. H., Li, X. S., and Rappenglueck, B.: CMAQ modeling and analysis of radicals,  
670 radical precursors, and chemical transformations, *J Geophys Res-Atmos*, 118, 11376-11387, Doi  
671 10.1002/Jgrd.50807, 2013.

672 Czader, B.H., Choi, Y., Li, X., Alvarez, S., Lefer, B.: Impact of updated traffic emissions on  
673 HONO mixing ratios simulated for urban site in Houston, Texas. *Atmos. Chem. Phys.*, 15(3),  
674 1253-1263, 2015.

675 Darby, L. S.: Cluster analysis of surface winds in Houston, Texas, and the impact of wind  
676 patterns on ozone, *Journal of Applied Meteorology*, 44, 1788-1806, 10.1175/jam2320.1, 2005.

677 Daum, P. H., Kleinman, L. I., Springston, S. R., Nunnermacker, L. J., Lee, Y. N., Weinstein-  
678 Lloyd, J., Zheng, J., and Berkowitz, C. M.: Origin and properties of plumes of high ozone  
679 observed during the Texas 2000 Air Quality Study (TexAQS 2000), *J Geophys Res-Atmos*, 109,  
680 Artn D17306 Doi 10.1029/2003jd004311, 2004.

681 Deng, A., Stauffer, D., Gaudet, B., Dudhia, J., Hacker, J., Bruyere, C., Wu, W., Vandenberghe,  
682 F., Liu, Y., Bourgeois, A.: Update on WRF-ARW End-to-end Multi-scale FDDA System. 10th  
683 WRF Users' Workshop, Boulder, CO, NCAR., 2009

684 Foley, K. M., Roselle, S. J., Appel, K. W., Bhawe, P. V., Pleim, J. E., Otte, T. L., Mathur, R.,  
685 Sarwar, G., Young, J. O., Gilliam, R. C., Nolte, C. G., Kelly, J. T., Gilliland, A. B., and Bash, J.  
686 O.: Incremental testing of the Community Multiscale Air Quality (CMAQ) modeling system  
687 version 4.7, *Geoscientific Model Development*, 3, 205-226, 2010.

688 Gilliam, R. C., and Pleim, J. E.: Performance Assessment of New Land Surface and Planetary  
689 Boundary Layer Physics in the WRF-ARW, *Journal of Applied Meteorology and Climatology*,  
690 49, 760-774, 10.1175/2009jamc2126.1, 2010.

691 Haman, C.L., Couzo, E., Flynn, J.H., Vizuet, W., Heffron, B., Lefer, B.L.: Relationship  
692 between boundary layer heights and growth rates with ground-level ozone in Houston, Texas. *J*  
693 *Geophys Res-Atmos* 119, 6230-6245, 2014.

694 Haman, C.L., Lefer, B., Morris, G.A.: Seasonal Variability in the Diurnal Evolution of the  
695 Boundary Layer in a Near-Coastal Urban Environment. *J Atmos Ocean Tech* 29, 697-710, 2012.

696 Huang, X.-Y., Xiao, Q., Barker, D. M., Zhang, X., Michalakes, J., Huang, W., Henderson, T.,  
697 Bray, J., Chen, Y., and Ma, Z.: Four-dimensional variational data assimilation for WRF:  
698 Formulation and preliminary results, *Monthly Weather Review*, 137, 299-314, 2009.

699 Kleinman, L. I., Daum, P. H., Lee, Y. N., Nunnermacker, L. J., Springston, S. R., Weinstein-  
700 Lloyd, J., and Rudolph, J.: Ozone production efficiency in an urban area, *J Geophys Res-Atmos*,  
701 107, Artn 4733 Doi 10.1029/2002jd002529, 2002.

702 Le Dimet, F.X. and Talagrand, O.: Variational algorithms for analysis and assimilation of  
703 meteorological observations: theoretical aspects, *Tellus*, 38A, 97-110, 1986.

704 Li, X., and Rappenglück, B.: A WRF-CMAQ study on spring time vertical ozone structure in  
705 Southeast Texas, *Atmospheric Environment*, 97, 363-385, DOI 10.1016/j.atmosenv.2014.08.036,  
706 2014.

707 Li, X., Lee, D., Kim, S.-T., Kim, H., Ngan, F., Cheng, F., and Byun, D.: Performance  
708 Evaluation of a Year-long Run of an Air Quality Forecasting System for Southeast Texas,  
709 10th Conference on Atmospheric Chemistry, New Orleans, January 2008, 2008.

710 Liu, Y., Bourgeois, A., Warner, T., Swerdlin, S., and Hacker, J.: An implementation of  
711 observation nudging-based FDDA into WRF for supporting ATEC test operations, 2005 WRF  
712 user workshop, Boulder, CO, 2005.

713 Liu, Y., Bourgeois, A., Warner, T., Swerdlin, S., and Yu, W.: An update on "observation  
714 nudging"-based FDDA for WRF-ARW: Verification using OSSE and performance of real-time  
715 forecasts, 2006 WRF user workshop, Boulder, CO, 2006.

716 Ngan, F., and Byun, D.: Classification of Weather Patterns and Associated Trajectories of High-  
717 Ozone Episodes in the Houston-Galveston-Brazoria Area during the 2005/06 TexAQS-II,  
718 Journal of Applied Meteorology and Climatology, 50, 485-499, DOI 10.1175/2010jamc2483.1,  
719 2011.

720 Ngan, F., Byun, D., Kim, H., Lee, D., Rappengluck, B., and Pour-Biazar, A.: Performance  
721 assessment of retrospective meteorological inputs for use in air quality modeling during TexAQS  
722 2006, Atmos Environ, 54, 86-96, DOI 10.1016/j.atmosenv.2012.01.035, 2012.

723 Olaguer, E. P., Rappengluck, B., Lefer, B., Stutz, J., Dibb, J., Griffin, R., Brune, W. H., Shauck,  
724 M., Buhr, M., Jeffries, H., Vizueté, W., and Pinto, J. P.: Deciphering the Role of Radical  
725 Precursors during the Second Texas Air Quality Study, Journal of the Air & Waste Management  
726 Association, 59, 1258-1277, Doi 10.3155/1047-3289.59.11.1258, 2009.

727 Otte, T. L.: The impact of nudging in the meteorological model for retrospective air quality  
728 simulations. Part I: Evaluation against national observation networks, Journal of Applied  
729 Meteorology and Climatology, 47, 1853-1867, 10.1175/2007jamc1790.1, 2008.

730 Pan, S., Choi, Y., Roy, A., Li, X., Jeon, W., and Souri, A.: Modeling the uncertainty of several  
731 VOC and inerts impact on simulated VOC and ozone in Houston, Texas, Atmos Environ, 120,  
732 404-416, 2015

733 Parrish, D. D., Allen, D. T., Bates, T. S., Estes, M., Fehsenfeld, F. C., Feingold, G., Ferrare, R.,  
734 Hardesty, R. M., Meagher, J. F., Nielsen-Gammon, J. W., Pierce, R. B., Ryerson, T. B., Seinfeld,  
735 J. H., and Williams, E. J.: Overview of the Second Texas Air Quality Study (TexAQS II) and the  
736 Gulf of Mexico Atmospheric Composition and Climate Study (GoMACCS), *J Geophys Res-*  
737 *Atmos*, 114, Doi 10.1029/2009jd011842, 2009.

738 Pour-Biazar, A., McNider, R. T., Roselle, S. J., Suggs, R., Jedlovec, G., Byun, D. W., Kim, S.,  
739 Lin, C. J., Ho, T. C., Haines, S., Dornblaser, B., and Cameron, R.: Correcting photolysis rates on  
740 the basis of satellite observed clouds, *J Geophys Res-Atmos*, 112, D10302  
741 10.1029/2006jd007422, 2007.

742 Rappengluck, B., Perna, R., Zhong, S. Y., and Morris, G. A.: An analysis of the vertical structure  
743 of the atmosphere and the upper-level meteorology and their impact on surface ozone levels in  
744 Houston, Texas, *J Geophys Res-Atmos*, 113, Doi 10.1029/2007jd009745, 2008.

745 Rappenglück, B., Lefer, B., Mellqvist, J., Czader, B., Golovko, J., Li, X., Alvarez, S., Haman,  
746 C., and Johansson, J., 2011: University of Houston Study of Houston Atmospheric Radical  
747 Precursors (SHARP), Report to the Texas Commission on Environmental Quality, August 2011,  
748 145 pp

749 Skamarock, W. C., Klemp, J. B., Dudhia, J., Gill, D. O., Barker, M., Duda, K. G., Huang, Y.,  
750 Wang, W., and Powers, J. G.: A description of the Advanced Research WRF Version 3, 1-113,  
751 2008.

752 Stauffer, D. R., and Seaman, N. L.: Use of 4-dimensional data assimilation in a limited-area  
753 mesoscale model .1. Experiments with synoptic-scale data, *Monthly Weather Review*, 118,  
754 1250-1277, 1990.

755 Stauffer, D. R., and Seaman, N. L.: Multiscale 4-dimensional data assimilation, *Journal of*  
756 *Applied Meteorology*, 33, 416-434, 1994.

757 Tucker, S. C., R. M. Banta, A. O. Langford, C. J. Senff, W. A. Brewer, E.J. Williams, B. M.  
758 Lerner, H. D. Osthoff, and R. M. Hardesty. : Relationships of coastal nocturnal boundary layer  
759 winds and turbulence to Houston ozone concentrations during TexAQS 2006. *Journal of*  
760 *Geophysical Research: Atmospheres*, 115, no. D10 (2010).

761 Willmott, C. J.: On the Validation Of Models, *Physical Geography*, 2, 184-194,  
762 10.1080/02723646.1981.10642213, 1981.

763 Zhong, S. Y., In, H. J., and Clements, C.: Impact of turbulence, land surface, and radiation  
764 parameterizations on simulated boundary layer properties in a coastal environment, *J Geophys*  
765 *Res-Atmos*, 112, Doi 10.1029/2006jd008274, 2007.

766

767

768 Table 1. Major WRF physics and FDDA Options, the numbers in the parentheses are the related  
769 settings in WRF namelist file.

WRF Version	V3.5.1
Microphysics	Lin et al Scheme (2)
Long-wave Radiation	RRTMG (4)
Short-wave Radiation	New Goddard scheme (5)
Surface Layer Option	Monin-Obukhov with CB viscous sublayer scheme (1)
Land-Surface Option	Unified Noah LSM (2)
Urban Physics	None
Boundary Layer Scheme	YSU (1)
Cumulus Cloud Option	Kain-Fritsch (1)
FDDA	Grid nudging on for all; Observation-nudging on for the OA case

770

771

772

773 Table 2. Major CMAQ Options, the text in the parentheses are the related settings in CMAQ  
774 build script.

CMAQ version	V5.0.1
Chemical Mechanism	cb05tucl_ae5_aq: CB05 gas-phase mechanism with active chlorine chemistry, updated toluene mechanism, fifth-generation CMAQ aerosol mechanism with sea salt, aqueous/cloud chemistry
Lightning NOx emission	Included by using inline code
Horizontal advection	YAMO (Yamartino) (hyamo)
Vertical advection	WRF omega formula (vwrf)
Horizontal mixing/diffusion	Multiscale (multiscale)
Vertical mixing/diffusion	Asymmetric Convective Model (ACM) version 2 (acm2)
Chemistry solver	EBI (Euler Backward Iterative) (ebi_cb05tucl)
Aerosol	AERO5 for sea salt and thermodynamics (aero5)
Cloud Option	ACM cloud processor for AERO5 (cloud_acm_ae5)
Boundary conditions	Default static profiles

775

776

777

778

779

780  
 781  
 782  
 783  
 784  
 785  
 786  
 787

Table 3 Statistics of surface T, U-wind and V-wind for three WRF simulations: N – data points; Corr – Correlation; IOA – Index of Agreement; RMSE – Root Mean Square Error; MAE – Mean Absolute Error; MB – Mean Bias; O – Observation; M - Model; O\_M – Observed Mean; M\_M – Model Mean; SD – Standard Deviation; Units for RMSE/MAE/MB/O\_M/M\_M/O\_SD/M\_SD: degree C

Surface temperature T										
Case	N	Corr	IOA	RMSE	MAE	MB	O_M	M_M	O_SD	M_SD
No-OA	41058	0.83	0.89	2.0	1.5	0.9	27.4	28.3	3.1	2.8
1Hr-OA	41058	0.94	0.97	1.0	0.8	0.0	27.4	27.4	3.1	3.1
Surface U wind										
Case	N	Corr	IOA	RMSE	MAE	MB	O_M	M_M	O_SD	M_SD
No-OA	43246	0.76	0.84	1.4	1.1	-0.6	-1.3	-1.9	1.6	1.9
1Hr-OA	43246	0.81	0.89	1.0	0.8	-0.3	-1.3	-1.6	1.6	1.6
Surface V wind										
Case	N	Corr	IOA	RMSE	MAE	MB	O_M	M_M	O_SD	M_SD
No-OA	43246	0.76	0.8	2.1	1.7	1.2	0.4	1.7	2.0	2.6
1Hr-OA	43246	0.80	0.89	1.2	0.9	-0.1	0.4	0.4	2.0	2.0

788  
 789

790 Table 4 Statistics of ozone for CMAQ simulations, see table 3 for column header information

Case	N	Corr	IOA	RMSE	MAE	MB	O_M	M_M	O_SD	M_SD
No-OA	33308	0.72	0.78	14.9	12.3	9.3	24.4	33.7	16.5	14.1
1Hr-OA	33308	0.73	0.83	13.8	11.0	6.1	24.4	30.6	16.5	17.4

791

792 Table 5 Statistics of ozone on 09/25/2013, all day and hour 0 to 13. Both correlation and index of  
 793 agreement are unitless. The red numbers indicate the three hours (07 CST to 09 CST) when the  
 794 ozone in 1Hr-OA case is significantly better than the No-OA case due to much improved winds.

		No-OA		1Hr-OA	
	N	Corr	IOA	Corr	IOA
Hr All	1150	0.79	0.86	0.81	0.88
0	48	0.04	0.30	0.40	0.46
1	43	0.20	0.24	0.36	0.30
2	48	0.14	0.25	0.35	0.35
3	48	0.19	0.30	0.32	0.35
4	48	0.27	0.36	0.31	0.35
5	47	0.24	0.36	0.28	0.37
6	47	0.33	0.38	0.35	0.37
7	48	0.06	0.39	0.29	0.47
8	48	0.09	0.43	0.53	0.63
9	47	0.05	0.41	0.55	0.74
10	47	-0.10	0.29	0.30	0.51
11	47	0.13	0.39	-0.07	0.36
12	49	0.09	0.38	0.25	0.40
13	49	-0.09	0.37	0.36	0.46

795